

This manuscript has been submitted to the Journal of Geophysical Research (JGR), Please note that the manuscript has been edited according to minor revisions of two editors and has been resubmitted. It has yet to be formally accepted for publication. Subsequent version of this manuscript may have slightly different content. If accepted, the final version of this manuscript will be available via it's DOI link.

Flow dynamics and tributary mouth bar formation at river confluences with high rates of tributary sediment supply

G. Moradi¹, C.D. Rennie², R. Cardot¹ and S.N. Lane¹

¹Institute of Earth Surface Dynamics, Université de Lausanne, CH1015 LAUSANNE, Switzerland

²Civil Engineering Department, University of Ottawa, OTTAWA, Canada
Corresponding author: Gelare Moradi (gelare.moradi@unil.ch)

Flow dynamics and tributary mouth bar formation at river confluences with high rates of tributary sediment supply

G. Moradi¹, C.D. Rennie², R. Cardot¹ and S.N. Lane¹

¹Institute of Earth Surface Dynamics, Université de Lausanne, CH1015 LAUSANNE, Switzerland

²Civil Engineering Department, University of Ottawa, OTTAWA, Canada

Corresponding author: Gelare Moradi (gelare.moradi@unil.ch)

Key Points:

- Angular momentum ratio rather than momentum ration may be a better means of classifying river junctions.
- Tributary-attached bars can lead to secondary circulation even at low angular momentum ratios.
- Coarse-grained tributary-attached bars may form from main channel rather than tributary sediment.

Abstract

River confluences influence the formation of secondary circulation, bed morphology, and associated feedbacks. With distance downstream through a drainage network, it becomes likely that the flow momentum of tributaries is lower than that of the main river, creating confluences with very low momentum ratio. However, the tributary may be able to supply significant quantities of sediment, especially in watersheds with high relief. High flow and sediment supply events in the tributary may decouple in time from those in the main river. The capacity of the main river to evacuate tributary-delivered sediment may occasionally be lower than the sediment delivery rate. The result is the formation of confluences with large tributary mouth bars that may influence confluence flow structures even when the tributary discharge has declined. There are no field examples measured to date for such confluences. Here, we report the first field data for three such river confluences, along the upper Rhône River, Switzerland. We combine aDcp measurements with the analysis of the provenance of sediments in the tributaries and main stem. We introduce the angular momentum ratio for confluence classification. The formation of tributary mouth bars and a scour hole was identified for the two junctions with significant tributary sediment supply. These bars were sufficient to introduce secondary circulation even at very low flow momentum ratios. The analysis of sediment provenance suggested that the origin of the bars was not necessarily the tributary but could be a consequence of the effects of the tributary upon main channel sediment routing.

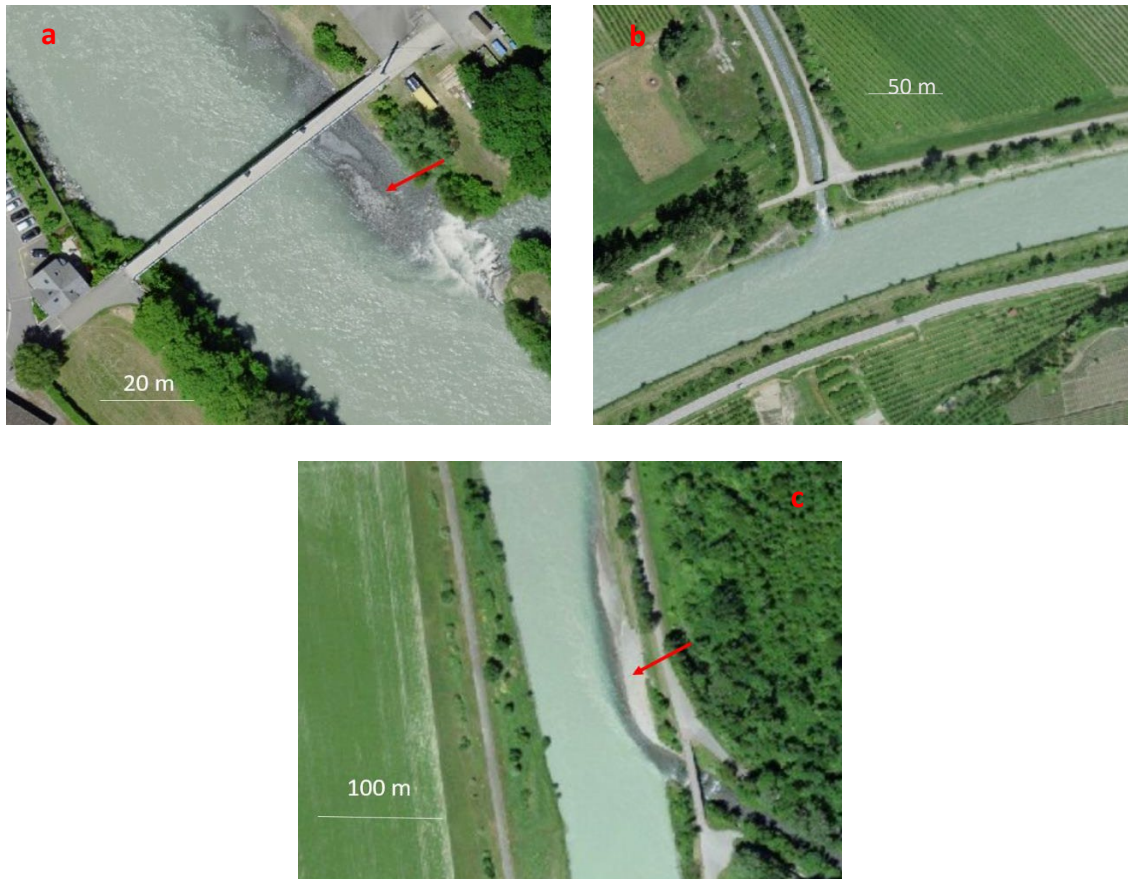
1 Introduction

Flow dynamics at the junction or confluence of two river channels is characterized by the formation of secondary flow. Extensive research has quantified this formation (e.g. Mosley, 1976; Best, 1987,1988; Rhoads and Kenworthy, 1995,1998; Biron, 1996; Biron et al., 1996a,1996b; Rhoads and Sukhodolov, 2001,2008; Rhoads et al., 2009; Constantinescu et al., 2011,2012; Leite Ribeiro, 2011; Konsoer and Rhoads, 2014; Lewis and Rhoads, 2015; Riley et al., 2015; Rhoads and Johnson, 2018; Yuan et al., 2021; Li et al., 2022) and attempted to establish what controls it. The momentum ratio (M_r):

$$M_r = \frac{Q_t U_t \rho_t}{Q_m U_m \rho_m} \quad (1)$$

43 where Q , U and ρ are discharge (m^3s^{-1}), mean flow velocity (ms^{-1}), flow density (kgm^{-3}), t and
44 m refer to the tributary and main channel, respectively; has been identified as a critical control
45 on the secondary circulation that forms. Its implications for the rate of mixing of the two
46 confluent channels and for stream bed erosion have been demonstrated (e.g. Kenworthy and
47 Rhoads, 1995; De Serres et al., 1999; Bradbrook et al., 2001; Lane et al., 2008; Rhoads et al.,
48 2009; Constantinescu et al., 2012; Riley and Rhoads, 2012; Riley et al., 2015; Lewis and
49 Rhoads, 2015; Rhoads and Johnson, 2018; Tang et al., 2018). There remain fewer studies of
50 how junction morphology evolves as M_r changes (but see Mosley, 1976; Ashmore and Parker,
51 1983; Best, 1988; Ashmore et al., 1992; Boyer et al. 2006; Rhoads et al., 2009). A dominant
52 but not exclusive focus on self-formed confluences in laboratory settings has described the
53 mutual adjustment between confluence morphology, flow processes and sediment transport.
54 However, and notably in large river basins, the timing of tributary sediment supply may not be
55 the same as in the main channel, leading to a disequilibrium between the tributary flow, the
56 main channel flow and the confluence morphology. High flow and sediment transport events in
57 the tributary may mean that for short time periods the tributary can deliver significant amounts
58 of coarse sediment to the main channel and/or influence the routing of main channel sediment
59 through the junction. Both can have geomorphological consequences, notably the formation of
60 a tributary mouth bar (e.g. Biron et al., 1993; De Serres et al., 1999) which may extend into the
61 main stem to form a bar attached to the downstream junction corner (Best, 1988; Guillén-
62 Ludeña et al., 2015, 2016, 2017; Leite Ribeiro et al., 2012). Although these are likely to be
63 formed during high flow events in the tributary, the bars themselves may remain in the main
64 stem for some time, leading to a confluence morphology that is not completely adjusted to M_r
65 values at low flows. This is particularly the case where steep tributaries enter main rivers, such
66 as in watersheds with a high relief, and the material can be very coarse. The associated deposits
67 may require shear stresses for entrainment substantially greater than those typical of the main
68 stem.

69
70 Figure 1 shows three examples of such confluences in the Swiss River Rhône. These tributary
71 mouth bars constrict the post confluence channel (Figure 1), causing the main stem to curve in
72 the same sense as the tributary. Thus, it is possible that even if the M_r between the tributary and
73 main stem is very low indeed, where there are “legacy” tributary mouth bars, secondary
74 circulation could form, and this could influence mixing and bed sediment transport through the
75 confluence, as well as the long-term stability of the tributary mouth bar itself.



76

77 Figure 1. Three examples of confluences in the Swiss River Rhône a. the Avançon; b. the
78 Lizerne and c. the Grande Eau. The Avançon and the Grande Eau have tributary mouth bars
79 attached to the downstream corner junction (annotated with red arrows) with sediment transport
80 in the tributary. Sediment delivery in the Lizerne is limited due to upstream hydropower
81 exploitation.

82 It is not clear whether these mouth bars form due to high sediment loading from the tributary
83 (Guillen Ludena et al., 2017); or from a high flow in the tributary that influences sediment
84 routing in the main stem, causing mouth bar formation from main stem sediment. The latter
85 may be encouraged due to discordance between the tributary and the main stem, such that the
86 tributary flow enters as a jet (Sukhodolov et al., 2017), with deceleration (Riley et al., 2015)
87 and upwelling of main stem flow downstream of the junction corner (Guillén-Ludeña et al.,
88 2016a).

89

90 Significant progress has been made in studying the hydraulics and morphodynamics of tributary
91 junctions with low momentum ratios but where there is a relatively high rate of sediment
92 delivery from the tributary (Leite Ribeiro et al., 2012; Guillén Ludena, et al., 2015; 2016; 2017).
93 These have predominantly focused on laboratory studies. There have been very few studies of
94 such junctions in field environments, notably where there is a low flow in the tributary, and no
95 sediment supply, leading to extremely low M_r (< 0.05). Leite Ribeiro et al. (2012) undertook
96 an experiment with $M_r = 0.02$ but a high rate of tributary-delivered, poorly-sorted sediment.
97 They showed that these conditions led to hydrodynamics that were different to existing
98 conceptual models. They concluded that the most unusual characteristic of confluences with
99 low momentum ratios and high rates of sediment supply is the formation of a pronounced bed
100 discordance in the confluence zone associated with the formation of a tributary mouth bar. The
101 discordance leads to a two layer-flow structure downstream of the junction. The flow from the

102 tributary mainly penetrates as a jet in the upper part of the water column. A horizontal
103 recirculation zone does not necessarily form downstream of the junction corner. Rather, the
104 main stem flow is accelerated under the tributary jet and then decelerates and upwells
105 downstream of the junction downstream corner (Guillén Ludena, et al., 2015). If the tributary
106 momentum decreases, the tributary mouth bar progrades into the main stem (Guillén Ludena,
107 et al., 2016) although this is in contrast to what others have observed (Best, 1998; Biron et al.,
108 1993; Riley et al., 2015). The height of the bank attached tributary mouth bar appeared to be
109 lower for higher momentum ratios (Guillén Ludena, et al., 2016).

110
111 Flow curvature from the tributary into the main channel will lead to a centrifugal force that is
112 not taken into account by consideration of momentum alone. For this reason, the centrifugal
113 force across the stream width should be integrated meaning the calculation of an angular
114 correction factor A . Herein, we introduce this factor to modify the momentum ratio to what is
115 effectively an angular momentum ratio (M_{ar}). The laboratory observations of Leite Ribeiro and
116 Guillén Ludena and their colleagues imply that the tributary mouth bars that form at confluences
117 with very low momentum ratios are going to relate to interactions between main stem and
118 tributary flow and sediment transport, which vary with flow stage. However, these processes
119 remain unclear and have yet to be observed in the field. Also, they did not consider the effect
120 of the angular momentum in correcting the momentum ratio. Accordingly, this paper tests three
121 hypotheses: (1) that due to the legacy of high tributary sediment delivery, tributary mouth bar
122 formation can lead to significant secondary circulation even at very low M_r conditions; (2) that
123 these tributary mouth bars form from both main flow and tributary supplied sediment; and (3)
124 the junction angle can lead to a centrifugal force that should be taken into account through a
125 corrected M_r .

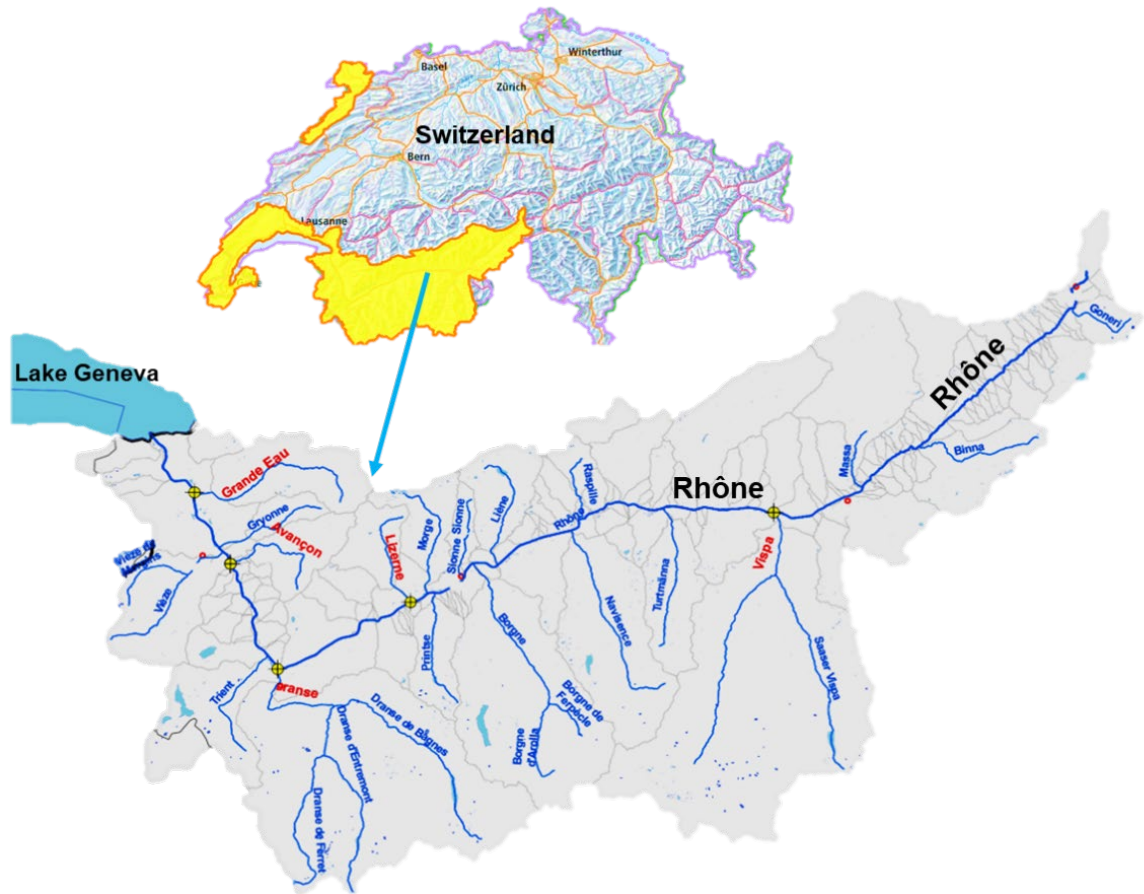
126 **1 Methodology**

127 The focus of the data collection is three junctions of the Swiss River Rhône. In this
128 section, we describe and justify the choice of these junctions and explain the measurements and
129 processing steps adopted.

130 **2.1 Study Site**

131 The tributaries are all in a sector of the river that has been extensively straightened for
132 flood control and each tributary is engineered to enter the main stem at a high angle (between
133 70° and 90°). Thus, they are not dissimilar to the design of laboratory experiments used to
134 inform some of our understanding of river confluence hydrodynamics (e.g. Best, 1987, 1988;
135 Biron et al., 1993; Leite Ribeiro et al., 2012; Guillén Ludena, et al. 2015, 2016). The three
136 tributaries were chosen on the basis of: (1) having low flow momentum ratios for most of the
137 time (< 0.05); (2) having high sediment supply rates in two cases, the third having a gravel trap
138 and sediment extraction upstream, negligible sediment supply and thereby providing a
139 controlled comparison; (3) high junction angles; and (4) suitability for sediment provenance
140 analyses so the origins of the sediment that comprised the tributary mouth bars could be
141 determined. The three junctions studied were: (1) the Avançon-Rhône confluence, (2) the
142 Lizerne-Rhône confluence and (3) the Grande Eau-Rhône confluence (Figure 2). The basic
143 characteristics of these three confluences are given in Table 1 and Figure 3.

144



145

146 Figure 2. Location of the three studied river confluences

Sites	Avançon	Lizerne	Grande Eau
Measurement date	16.10.2017	07.08.2017	23.05.2018
Tributary upslope contributing area (km ²)	87.5	64.8	132
Main stem upslope contributing area (km ²)	4402	3401	5088
Basin area ratio	1.99%	1.89%	2.59%
Tributary width (m)	8.5	6.5	16.5
Main stem width upstream of junction (m)	54	40	58
Main stem width downstream of junction (m)	56	52	60
Width ratio	0.18	0.15	0.28
Tributary mean depth at the junction (m)	0.2	1.4	0.8
Main stem mean depth upstream of junction (m)	1.5	1.9	2.4
Main stem mean depth downstream of junction (m)	3.1	2.5	3.5
Junction angle (°)	90	80	70
Tributary Froude number (Leite Ribeiro, 2011)	0.56	0.32	0.15
Bed slope of the tributaries upstream of the confluence (%) (Leite Ribeiro, 2011)	<1.5	~0.5	0.5-1
Main stem slope upstream of the confluence (%)	0.9	2	2.2
Tributary slope at discordant bed into main stem (°)	29.8	33.1	26.6
Discharge ratio during measurement	0.018	0.012	0.027
Momentum ratio during measurement	0.021	0.018	0.022
Radius of main channel curvature (°) (see section 2.4)	60.3	46.5	76.5
Angular momentum ratio during measurement (see section 2.4)	0.019	0.015	0.017

147

148 Table 1. Selected upper Rhône tributaries with their typical characteristics on the day of
149 measurements.

150

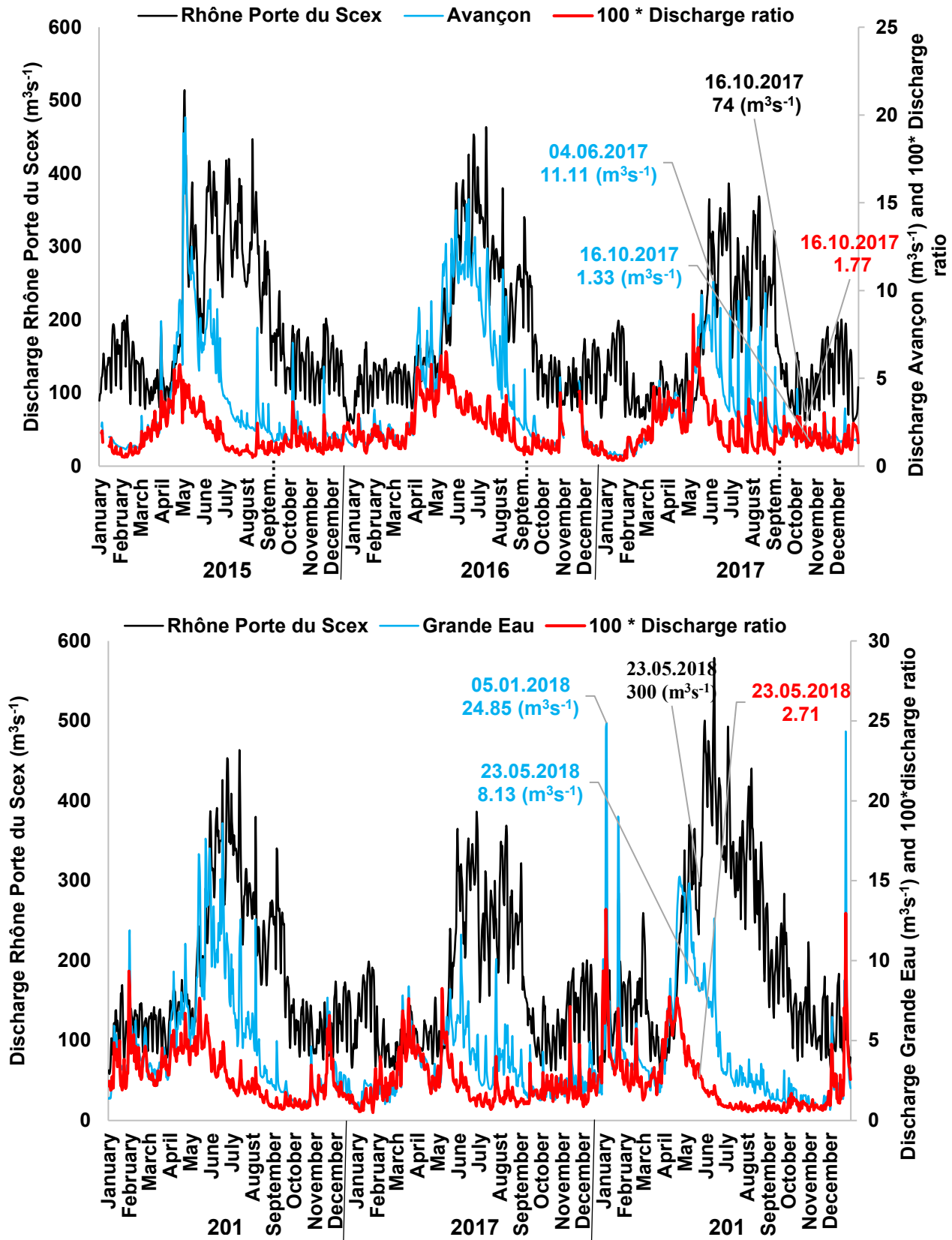
151 Figure 3 shows the historical daily mean discharge values for a period of 3 years for the
152 Avançon (Figure 3a) and the Grande Eau (Figure 3b). The values of daily mean discharges for
153 the measurement dates for both confluences are indicated on the graphs. As compared with the
154 measurement dates (Table 1) the last likely tributary-dominant event for the Avançon (Figure
155 3a) was on June 4th, 2017, with a discharge of 11.1 m³s⁻¹. The measurement duration of the
156 Avançon is too short to estimate a return period for the June 2017 event, but the closest rain
157 gauge suggests that the daily rainfall on the 4th of June was higher than 95.8% of daily rainfalls
158 in the period 1998-2018. This confluence was measured on the 16th August 2017 (Figure 4a)
159 when the momentum ratio according to (1) was 0.021.

160

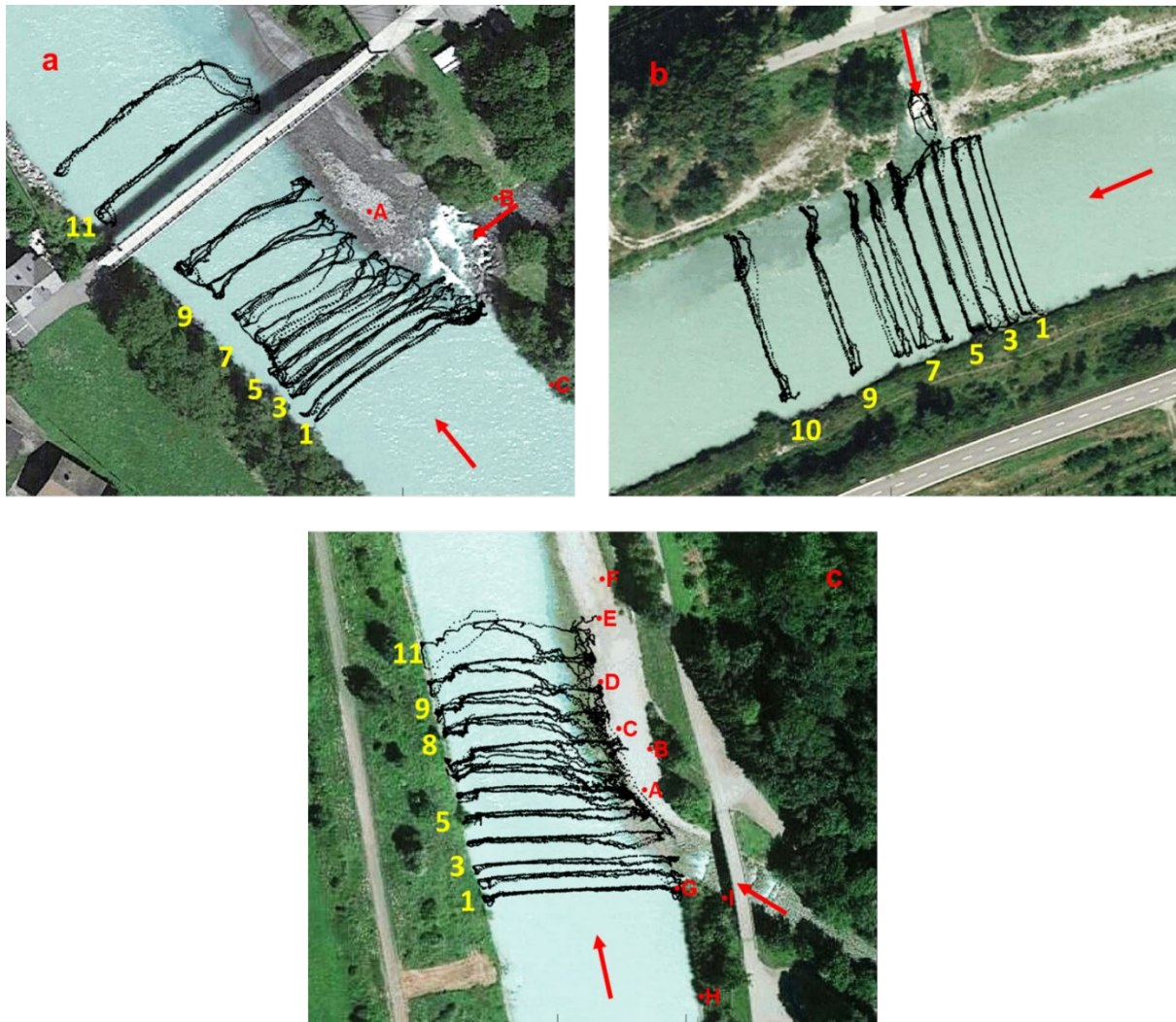
161 The Lizerne (Figure 4b) is heavily regulated for hydropower with sediment extracted upstream
162 of the junction (~3 km upstream of the junction). As a result, there is negligible sediment supply
163 and no evidence of tributary mouth bar formation. Field data were collected on August 7th, 2017
164 with an M_r of 0.018. There are no historical hydrological data for the tributary.

165

166 For the Grande Eau the last likely event before the date of measurement was January 5th, 2018
 167 (Figure 3b), with a discharge value of $24.9 \text{ m}^3\text{s}^{-1}$ and a return period of around 2 years (Source
 168 OFEV). The confluence was measured on the 23rd May 2018 when M_r was 0.022 (Figure 4c).



171 Figure 3. Daily mean discharge values for the Avançon (3a) in 2017 and the Grande Eau (3b)
 172 in 2018 (Source OFEV) with their discharge ratios. The Lizerne discharge is not measured.



173

174 Figure 4. Location and surveyed cross sections at a) Avançon-Rhône confluence (October
 175 2017), b) Lizerne-Rhône confluence (August 2017) and c) Grande Eau- Rhône confluence
 176 (May 2018) and selected cross sections for primary and secondary flows representation. Red
 177 points are the sediment samples
 178

179

2.2 Angular momentum ratio calculation

180 The calculations for momentum ratio presented in Section 2.1 were based upon (1).
 181 However, they have different junction angles (Figure 4). Theoretical analyses show that the
 182 intensity of secondary circulation in a river is influenced by curvature (Dietrich and Smith,
 183 1983) and hence as junction angle changes, so the degree of curvature changes. To allow better
 184 comparison we here introduce the angular momentum ratio. The angular momentum
 185 ratio is based upon taking into account the centrifugal force which is produced by the curvature
 186 of the flow from the tributary into the main channel. For this reason, the angular correction
 187 factor (A) is calculated for all three tributaries by integrating the centrifugal force across the
 188 stream width (W) using:

$$A = \frac{r_1}{r_2} \quad (2)$$

189 where r_1 and r_2 are the radii of the main channel curvature (m) and tributary curvature
 190 respectively. If each channel has curvature at the confluence mixing zone, then r_1 and r_2 in

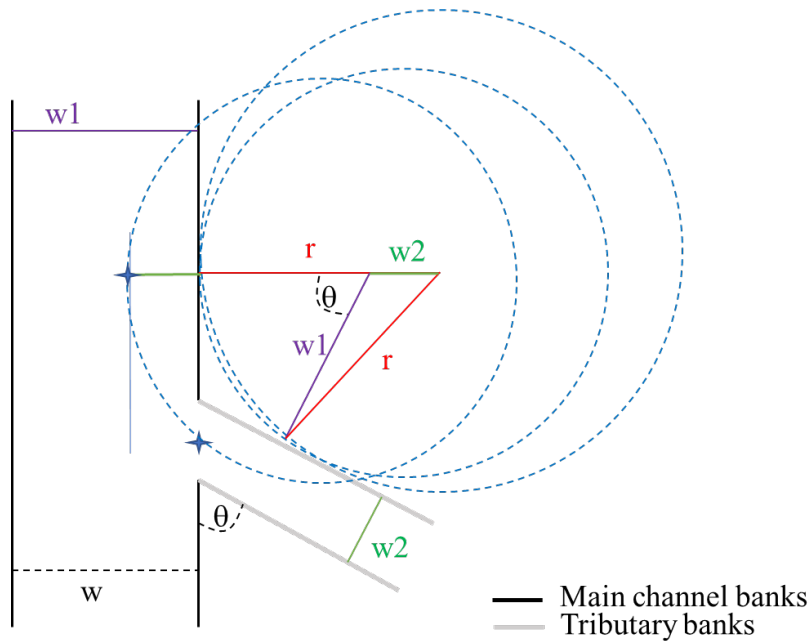
191 equation 2 should be perpendicular to the flow path of the respective channel. As the main
 192 channel is straight at all three junctions, r_1 tends to infinity. To be able to compare these three
 193 confluences, it is assumed that r_1 is equal to the width of the main channel upstream of the
 194 junction (w) and the correction is only applied to the tributaries. Applying (2) needs
 195 determination of r_2 on the basis of the junction angle (θ). Whilst the junction angle is readily
 196 measurable, the radius of curvature can only be determined from the junction angle if there is
 197 some length scale specified over which the tributary must turn. It is argued here that this length
 198 scale should be based upon the width of the main channel downstream of the junction (W_1) and
 199 the width of the tributary (W_2) (see Figure 5).
 200

$$r_2 = \sqrt{W_1^2 \times W_2^2 - 2 \times W_1 \times W_2 \times \cos(180 - \theta)} \quad (3)$$

201
 202 This ratio then is used to obtain the angular momentum ratio (M_{ar}):

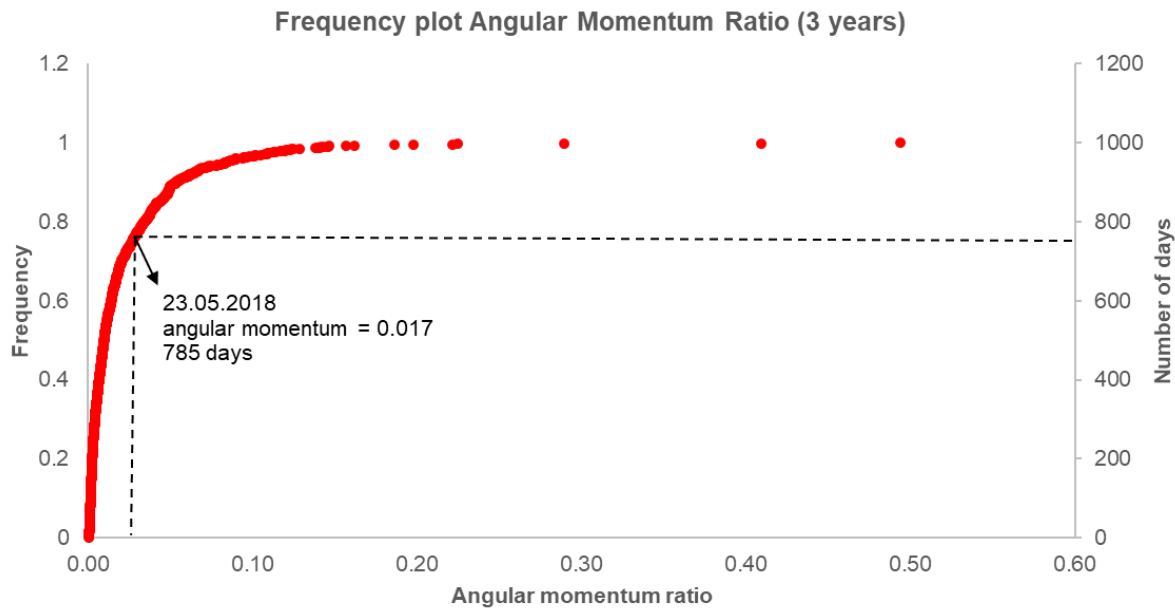
$$M_{ar} = A \times M_r \quad (4)$$

203
 204 Table 1 gives the angular momentum ratio, showing how this correction increases the
 205 momentum ratio in the Avançon and the Lizerne as compared with the Grande Eau. This is due
 206 to the smaller junction angle at the Grande Eau which leads to a smaller penetration of the
 207 tributary into the main channel.
 208



209
 210
 211 Figure 5. Schematic of angular momentum calculation

212 Angular momentum ratios for the Grande Eau from 2016 to 2018 can be calculated by applying
 213 the angular factor to correct the momentum ratios determined using historical water level data,
 214 assuming that the section is rectangular, so the width is constant. Figure 6 shows the frequency
 215 plot of the calculated angular momentum ratio. A similar analysis was not possible for the
 216 Avançon junction due to only discharge data being available.
 217



218
219 Figure 6. Frequency plot for angular momentum ratio for the Grande Eau from 2016 to 2018

220 2.3 Velocity and bathymetric data collection

221 At each confluence, the measurement of the bathymetry and the time-averaged flow
222 velocities and flow discharge at several cross sections through the confluence was performed
223 using a moving boat acoustic Doppler current profiler (aDcp) system. This system has proven
224 to be a reliable means of estimating the mean discharge and velocity in rivers. This method can
225 be used not only to estimate the discharge (e.g., Parsons et al., 2005; Kostaschuk et al., 2009;
226 Gunawan et al., 2010; Shugar et al., 2010; Sassi et al., 2011) but also local bed shear stress (τ)
227 (e.g., Sime et al., 2007; Petrie et al., 2010; Rennie and Church 2010), sediment transport (e.g.,
228 Gartner, 2004; Rennie and Villard, 2004; Rennie and Millar, 2004; Kostaschuk et al., 2005;
229 Parsons et al., 2005) and secondary circulation (Dinehart and Burau, 2005; Szupiany et al.
230 2007; Venditti et al. 2014). The aDcp was a Sontek RiverSurveyor M9, which sets beams at
231 25° angle from vertical. It was trimaran mounted and synchronized with a differential Global
232 Positioning System (dGPS). This system has a profiling range of 0.06 to 40m and can measure
233 a velocity range of $\pm 20 \text{ ms}^{-1}$ in vertical bin cell sizes ranging from 0.02 to 4 m. The aDcp
234 measurements of depth and velocity were made in single ping ensembles using 10 cm long bins.
235

236 A specially-designed rope pulley system (Figure 7) was set up for cross-sections, each
237 perpendicular to the main Rhône with a $0.1w$ spacing (w is the post confluence river channel
238 width) to a distance $2w$ downstream of the downstream junction corner. It is impossible to
239 maintain even partly straight lines with a motorized boat in this kind of stream. Figure 4 shows
240 that certainly for the Avançon (Figure 4a) and the Lizerne (Figure 4b) it was possible to use the
241 pulley to reproduce the same traverse of each section. For the Grande Eau (Figure 4c), due to
242 the distances involved, coupled to the increased width of the main stem, this was less the case,
243 and this may introduce some error into the Grande Eau results. Following the recommendations
244 of Szupiany et al. (2007), the cross-sectional measurements were made by conducting six
245 traverses along each cross section.
246



247

248 Figure 7. Rope-pulley system, illustrated for the Lizerne

249 2.4 Velocity and bathymetric data processing

250 The aDcp data collected at each confluence were first processed to yield spatially-distributed
 251 maps of bathymetry, near-surface velocity, and near-bed velocity. The water depth and profile
 252 of three dimensional (3D) Cartesian velocities (east, north, and up components) collected at all
 253 aDcp measurement points were extracted and processed in Matlab. Along with the water depths,
 254 the east and north velocity vector components and the 3D velocity magnitude in the bins nearest
 255 the water surface and nearest the bed were then interpolated using Kriging in Surfer software
 256 to generate spatial maps of these quantities.

257

258 Secondary flow circulation at individual transects was identified using the beam velocity
 259 method (Vermeulen et al. 2014b) aided by the repeat surveys of each transect (Figure 4). A full
 260 description and evaluation of this method is given in Moradi et al. (2019) and only a brief
 261 explanation is provided here. An aDcp measures the radial beam velocities (\mathbf{b}), i.e., the
 262 projections of the local velocity vectors in the direction of each acoustic beam (\mathbf{q}). To determine
 263 Cartesian velocity components (v_x , v_y and v_z), these radial velocities have to be resolved into
 264 three orthogonal velocity vectors. These velocities should then be corrected for pitch and roll
 265 angles, obtained from the aDcp's internal inclinometer and heading angle from the aDcp's
 266 internal compass. The method introduced by Vermeulen et al. (2014b) was used to transform
 267 radial beam velocities measured within a velocity bin to Cartesian velocity components, using
 268 the following equation:

269

$$\begin{pmatrix} b_1 \\ \vdots \\ b_N \end{pmatrix} = \begin{pmatrix} q_1 \\ \vdots \\ q_N \end{pmatrix} \cdot \begin{pmatrix} v_x \\ v_y \\ v_z \end{pmatrix} \leftrightarrow \mathbf{b} = \mathbf{Q} \cdot \mathbf{u} \quad (5)$$

270

271

272 Since there is always some measurement error due to instrument noise, the above equation can
 273 be rewritten as:

274

$$\mathbf{b} = \mathbf{Q}\mathbf{u} + \varepsilon \quad (6)$$

275
276
277
278

where ε is the error term. A least squares solution can be then fitted to (6) that minimizes the sum of the square of the errors. The optimal velocity estimation (\hat{u}) for (\vec{u}) is then given by the normal equation:

$$\hat{u} = Q^+ \mathbf{b} + \varepsilon \quad (7)$$

279
280
281
282

The error term also includes information about the turbulence and accuracy of the measurements. The covariance matrix of the velocity components can be obtained using the following equations:

$$\hat{\varepsilon} = \mathbf{b} - Q\hat{u} \quad (8)$$

283

$$var(\hat{u}) = \frac{\hat{\varepsilon}^T \hat{\varepsilon} (Q^T Q)^{-1}}{N - 3} \quad (9)$$

284
285
286

and the variance of the velocity across the section can then be estimated as:

$$var(u) = \frac{var(\hat{u})}{N} \quad (10)$$

287

288 As the instrument is mounted on a moving boat, corrections should be made for boat velocity
289 in order to obtain absolute water velocities. The boat velocity is determined either by bottom
290 tracking (BT) or by use of differential Global Positioning System (dGPS) data. Boat velocity
291 measurement by bottom tracking is typically more accurate than by dGPS, but bottom tracking
292 for water velocity measurement is limited to immobile bed conditions. Bottom tracking
293 involves measurement of the Doppler shift in the frequency of an independent echo sounding
294 off the bed. If the bed is stationary, the shift in frequency is proportional to the boat velocity.
295 However, if the bed is mobile then bottom tracking is biased by the sediment motion and the
296 frequency shift is due to both the boat velocity and the sediment motion. In this study, the boat
297 velocity measured by dGPS is used because of the possibility of the bed being mobile.

298

299 The basic bathymetric model is estimated using the UTM positioning of the bed elevation data
300 collected with the aDcp and a LOWESS interpolation model (Moradi et al. 2019), which has
301 the effect of defining a bathymetric model that gives most weight to points that appear to be
302 closer to the measured points. For each cross section, a best-fit section line is also defined using
303 the UTM positions of the bed elevation of all six repeat transects, estimated using the
304 bathymetric model. Using this best fit cross-section, a cross-section mesh is then generated and
305 measured beam velocities are projected onto this mesh. Cartesian velocity components are then
306 calculated for each mesh cell using the procedure defined above. The beam velocity processing
307 method yielded calculated Cartesian velocities at each point in the cross-section mesh. Moradi
308 et al. (2019) has used the same approach for the Avançon and the Lizerne and has reported that
309 using this new method improves significantly the results obtained for secondary circulations.
310 Primary and secondary velocity vectors were then estimated, based on the assumption that the
311 secondary currents in one direction are balanced by those in opposite direction, to produce zero
312 secondary discharge for a given profile. Finally, the secondary velocities were evaluated for the
313 presence of helical cells. At the confluence of two rivers, the large-scale helical cells can interact
314 and form the smaller scale secondary circulation cells within their mixing interface. These
315 small-scale helixes are known as streamwise oriented vertical (SOV) cells (Sukhodolov and
316 Sukhodolova, 2019)

317

318 2.5 Analysis of sediment provenance

319 The study was interested not only in the flow structures that formed in the presence of
 320 tributary mouth bars at very low flows, but also the origin of the tributary mouth bars
 321 themselves. Reflecting the severe difficulty of measuring coarse sediment transport in the
 322 junction during extreme tributary flows, the study sought to attribute tributary mouth bar
 323 formation to sediment sourced from the tributary versus sediment sourced from the main stem,
 324 as this would allow inference of possible sediment transport paths during tributary mouth bar
 325 formation.

326
 327 The upper Rhône River basin comprises three litho-tectonic units with different geological
 328 histories (Stutenbacker et al., 2018). The External Massifs include autochthonous slices of
 329 crystalline basement (Herwegh et al., 2017) as well as some “sub-penninic” (i.e. allochthonous)
 330 basement nappes containing mostly metagranites and gneisses (Stutenbacker et al., 2018). The
 331 Penninic nappes include: (1) ophiolites of the Valais and Piedmont-Liguria oceans
 332 (metabasalts, metagabbros, serpentinites, calcschists, flysch sediments); and (2) gneisses and
 333 micashists from the Briançonnais continent (Stutenbacker et al., 2018). The Helvetic nappes
 334 comprise mostly carbonates from a passive margin setting (Stutenbacker et al., 2018).
 335 Stutenbacker et al. (2018) modelled the relative importance of these three sources to sediment
 336 delivered to Lake Geneva through the analysis of sediment provenance. They estimated that
 337 $56.9\% \pm 9.6\%$ of sediment comes from the External Massifs, $23.4\% \pm 2.3\%$ from the Penninics
 338 and $19.7\% \pm 1.0\%$ from the Helvetics, and also calculated these proportions for a site upstream
 339 of the Avançon confluence with the Rhône and upstream of the Grand Eau confluence of the
 340 Rhône. The Avançon is almost exclusively underlain by Helvetics high in CaO (Table 2). The
 341 Grande Eau contains Helvetics and Penninics (Table 2). The two Rhône sites are relatively
 342 similar despite tributary inputs because at this distance downstream the tributary areas, and
 343 hence sediment supply rates, are much lower than the main Rhône. Thus, the Avançon and the
 344 Grande Eau have very different sediment sources in geological terms as compared with the main
 345 Rhône itself.

346
 347
 348

	Avançon	Rhône at Avançon junction ¹	Grande Eau	Rhône at Grande Eau junction ¹
Penninics	Area: 0%	27%	68%	27%
External massifs	0%	55%	0%	57%
Helvetics	100%	18%	32%	16%
SiO ₂	30.8%	58.6%	Not measured	56.0%
CaO	27.5%	12.2%	Not measured	11.4%

349
 350 Table 2. Relative contribution of litho-tectonic units to the sediment at Avançon-Rhône and
 351 Grande Eau-Rhône confluences. (1) indicates data from calculations in Stutenbacker et al.
 352 (2018). SiO₂ and CaO data are from Stutenbecker et al. (2018)

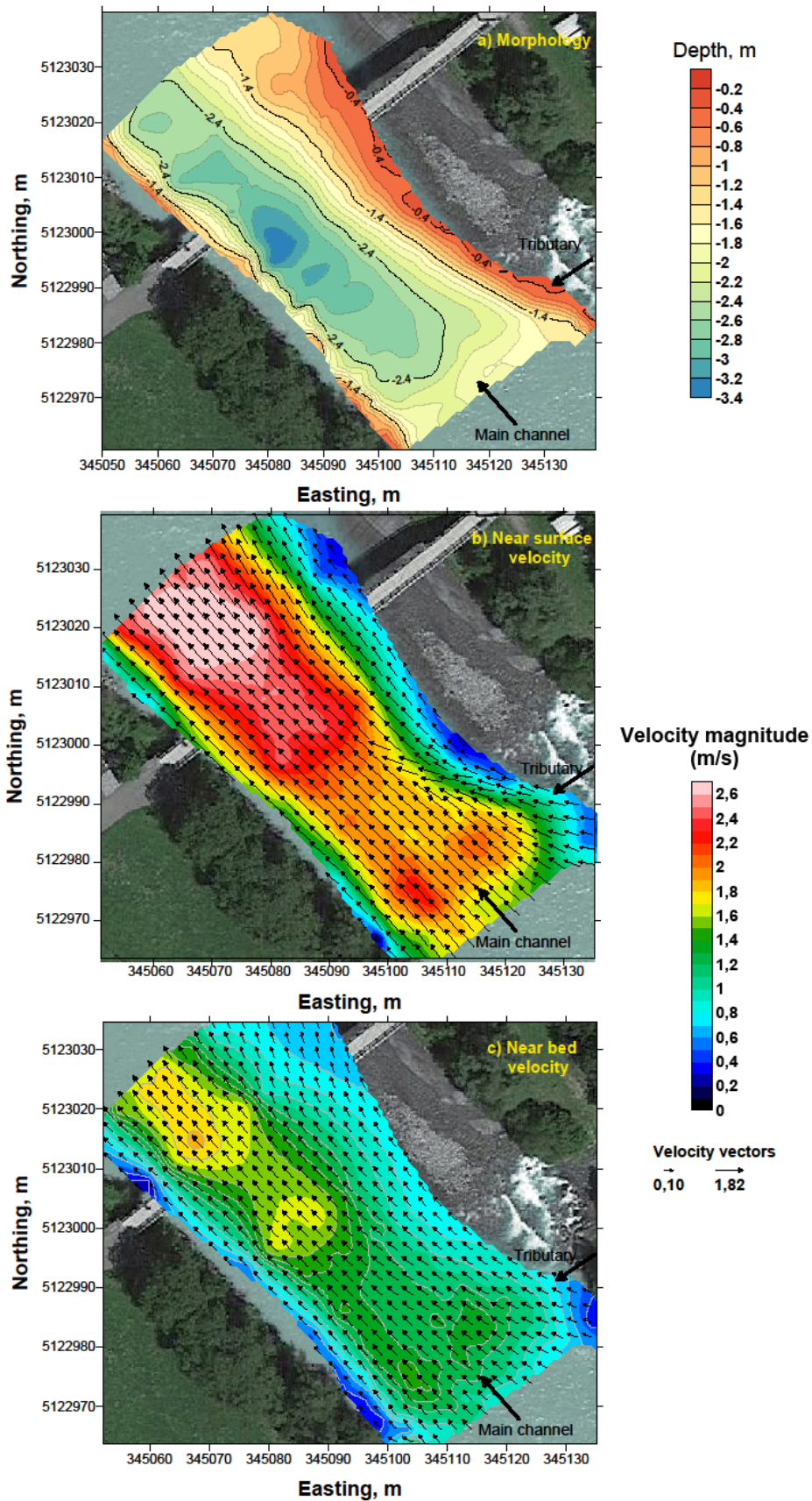
353 This study used these differences in sediment provenance to identify where sediment deposited
 354 in the tributary mouth bars is likely to originate. Bed sediment samples were collected at
 355 locations within the mouth bar as well as within the tributary and upstream of the junction in
 356 the main stem (Figure 4). During measurement, access allowed more sites to be sampled for the
 357 Grande Eau than for the Avançon. In order to validate our methods, we included three of the

358 sites measured by Stutenbacker et al. (2018): in the Rhône upstream of the Avançon and the
359 Grande Eau respectively, and in the Avançon. Stutenbacker et al. did not measure the Grande
360 Eau. At each sample location we sampled at a number of sediment depths.
361 The samples were prepared and crushed in the laboratory to obtain a homogenous dry powder
362 which were then calcined and mixed with Lithium-Tetraborat powders. A total of 1.2g of these
363 powders was used to prepare fused-disks for each sample. These disks were then analysed in
364 the laboratory using X-ray florescence (XRF) spectrometry to identify and quantify their major
365 chemical elements (SiO_2 , TiO_2 , Al_2O_3 , Fe_2O_3 , MnO , MgO , CaO , Na_2O , K_2O , P_2O_5 , Cr_2O_3 ,
366 NiO). XRF is capable of measuring elements in concentrations from ppm level up to 100wt%
367 and of identifying high- SiO_2 and low- SiO_2 and carbonate rocks.
368
369

370 **3 Results**

371 3.1 Bed morphology and surface and near-bed planform velocities

372 Figure 8 shows the bathymetry and near surface and near bed velocity vectors, obtained
373 for the Avançon–Rhône confluence with $Mar=0.019$. The bathymetry (Figure 8a) shows the
374 presence of bed discordance with the tributary higher than the main channel. Because of this
375 discordance, flow from the tributary enters the main channel only in the upper part of the water
376 column and forces water at the surface towards the outer bank (Figure 8b). The main-channel
377 flow is not influenced by the tributary in the lower part of the water column (Figure 8c), which
378 implies a two-layer flow structure at the tributary mouth. The tributary mouth bar, which
379 extends down the tributary side of the main Rhône, reduces the main channel width by almost
380 30% and leads to flow acceleration at both the surface (Figure 8a) and the bed (Figure 8b). At
381 about 0.5 multiples of the main stem width downstream from the tributary, the apex of the
382 tributary mouth bar has been passed and the main channel flow expands, even as it continues
383 to accelerate. Near the bed (Figure 8c), there is also flow acceleration but both the tributary and
384 the tributary mouth bar seem to have less effect upon the flow. The net result of the tributary
385 and its mouth bar is curvature of the flow in the main channel. Whether due to flow acceleration
386 (Figure 8b) or secondary circulation (see below) there is evidence of scour, displaced to the true
387 left of the main Rhône (Figure 8a). The bridge had no piers, but it did narrow the channel very
388 slightly (about 5%). As the Froude number during measurement was 0.56 it is unlikely that the
389 measured flows are influenced by this.



390

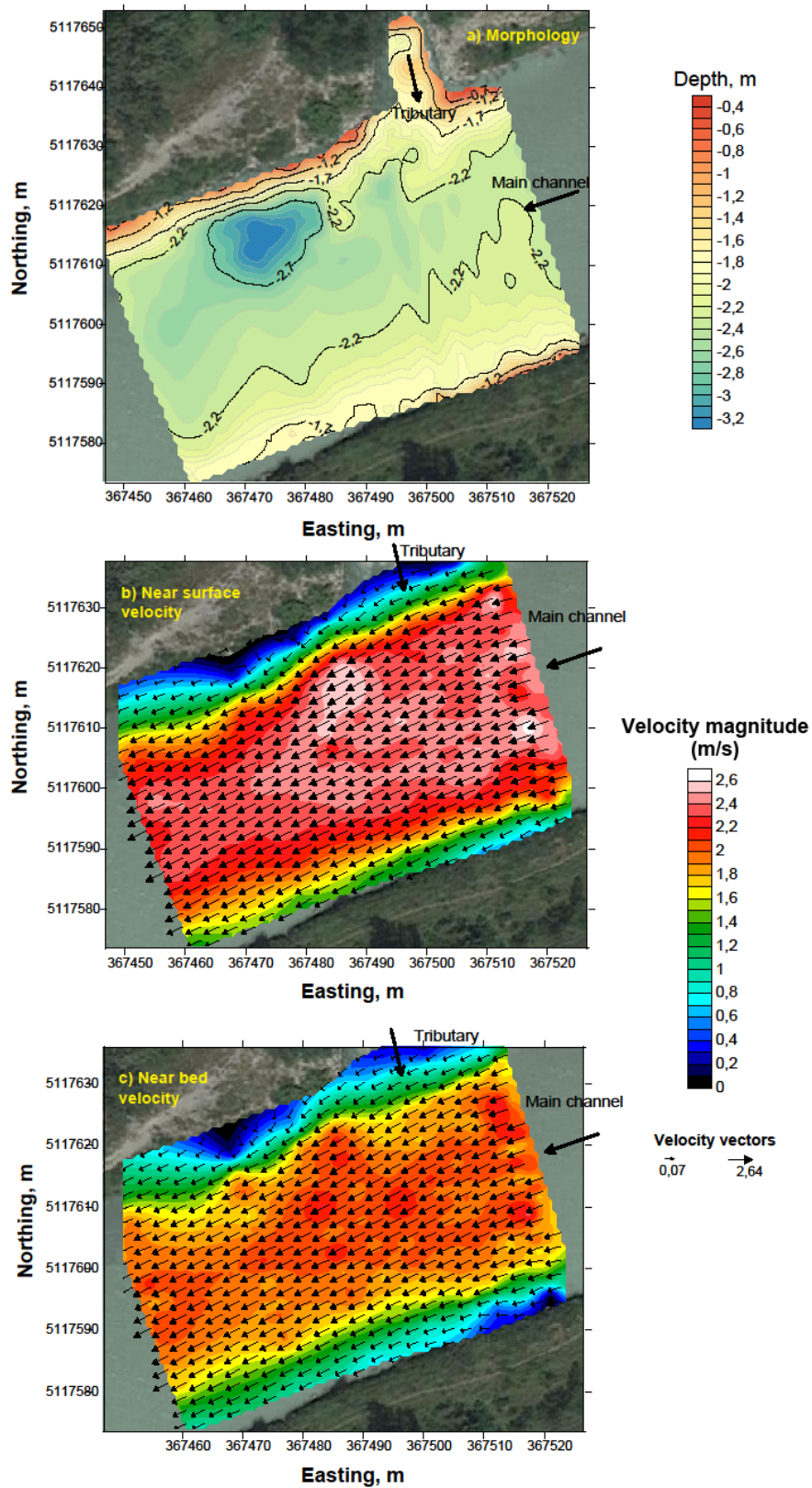
391 Figure 8. Avançon-Rhône confluence: patterns of morphological changes (a) and planform

392 velocity vector distributions from moving ADCP measurement close to the free surface (b) and

393 near the bed (c) and velocity magnitudes (contours in b & c).

394 The results obtained for Lizerne-Rhône confluence (Figure 9a) are different to those for the
395 Avançon-Rhône. The bed is concordant, there is no tributary mouth bar and there is a scour
396 hole near the inner bank (Figure 9a). The angular momentum ratio was slightly lower than the
397 Avançon during measurement (0.015 rather than 0.019) but there is no evidence of tributary
398 penetration into the main flow, at either the surface (Figure 9b) or the bed (Figure 9c), nor of
399 flow acceleration or deceleration. The presence of the scour hole suggests that there are
400 conditions that lead the tributary to have a morphodynamic impact upon the main channel
401 bathymetry, but that the main river is able to preserve the associated scour hole once developed.

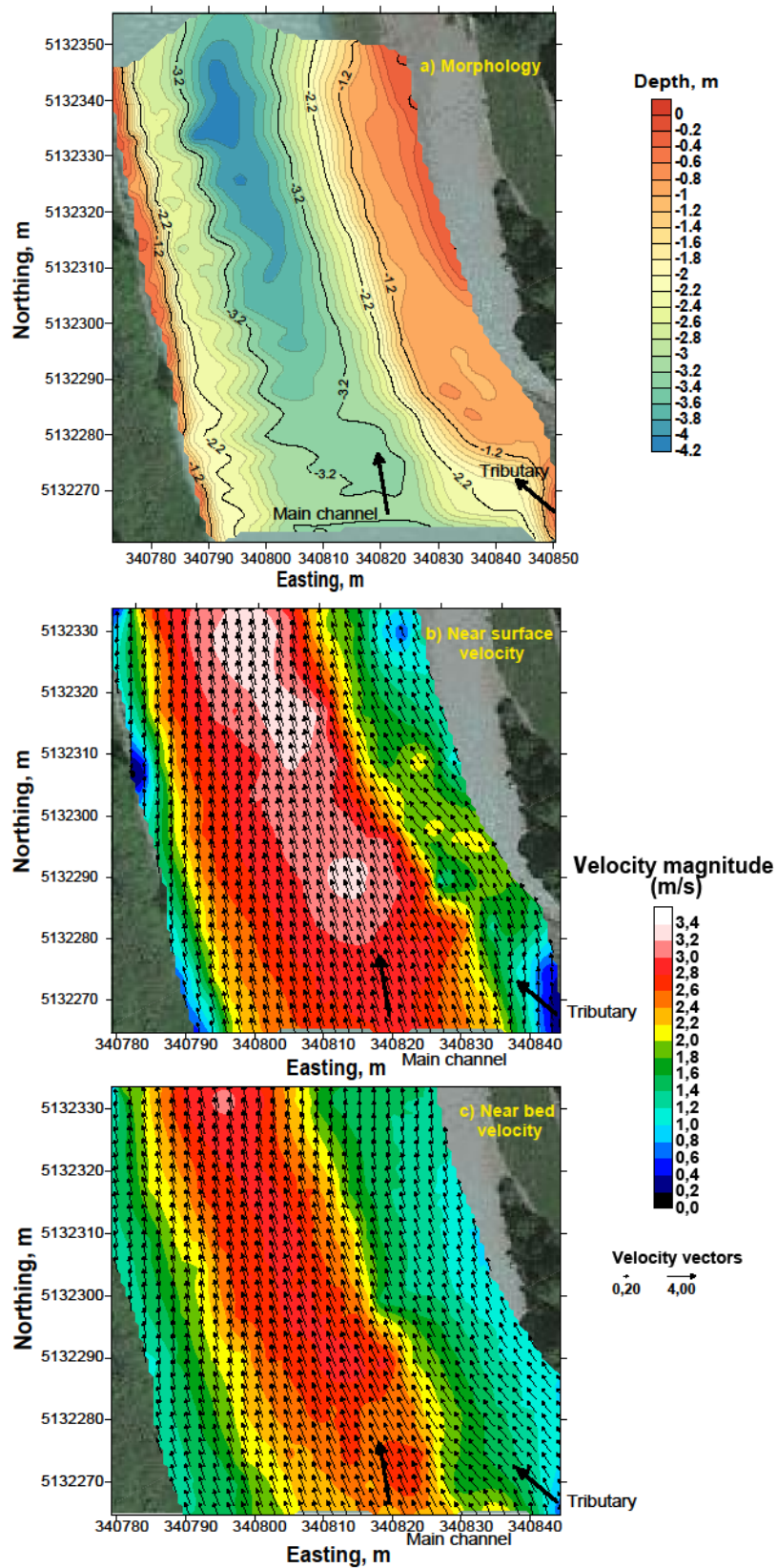
402



403

404 Figure 9. Lizerne-Rhône confluence: patterns of morphological changes (a) and depth-averaged
 405 streamwise velocity vector distributions from moving ADCP measurement close to the free
 406 surface (b) and near the bed (c) and velocity magnitudes (contours in b & c)

407 The Grand Eau-Rhône confluence has a discordant bed (Figure 10a) and the tributary meets the
408 main stem flow in the upper part of the water column. There is some evidence of a scour hole
409 but this is found more towards the centre of the main channel and downstream, as compared
410 with the Avançon (Figure 10a). There is a tributary mouth bar, and this extends from about half
411 way across the tributary and well down into the main channel (Figure 10a). The bar appears to
412 have two distinct surfaces, at about 1 m depth starting at the tributary mouth, and then with a
413 higher zone starting from Northing 5132305 m. The velocity vectors in Figure 10b suggest
414 reduced penetration of the Grande Eau into the Rhône as compared with the Avançon, although
415 there appears to be some surface flow deflection at the tributary mouth at the surface. Flow then
416 returns to the right (i.e. tributary bank) before a second zone of deflection around the higher
417 zone of the bar further downstream. There is evidence of flow constriction and acceleration of
418 the surface flow (Figure 10b) but less so at the bed (Figure 10c).



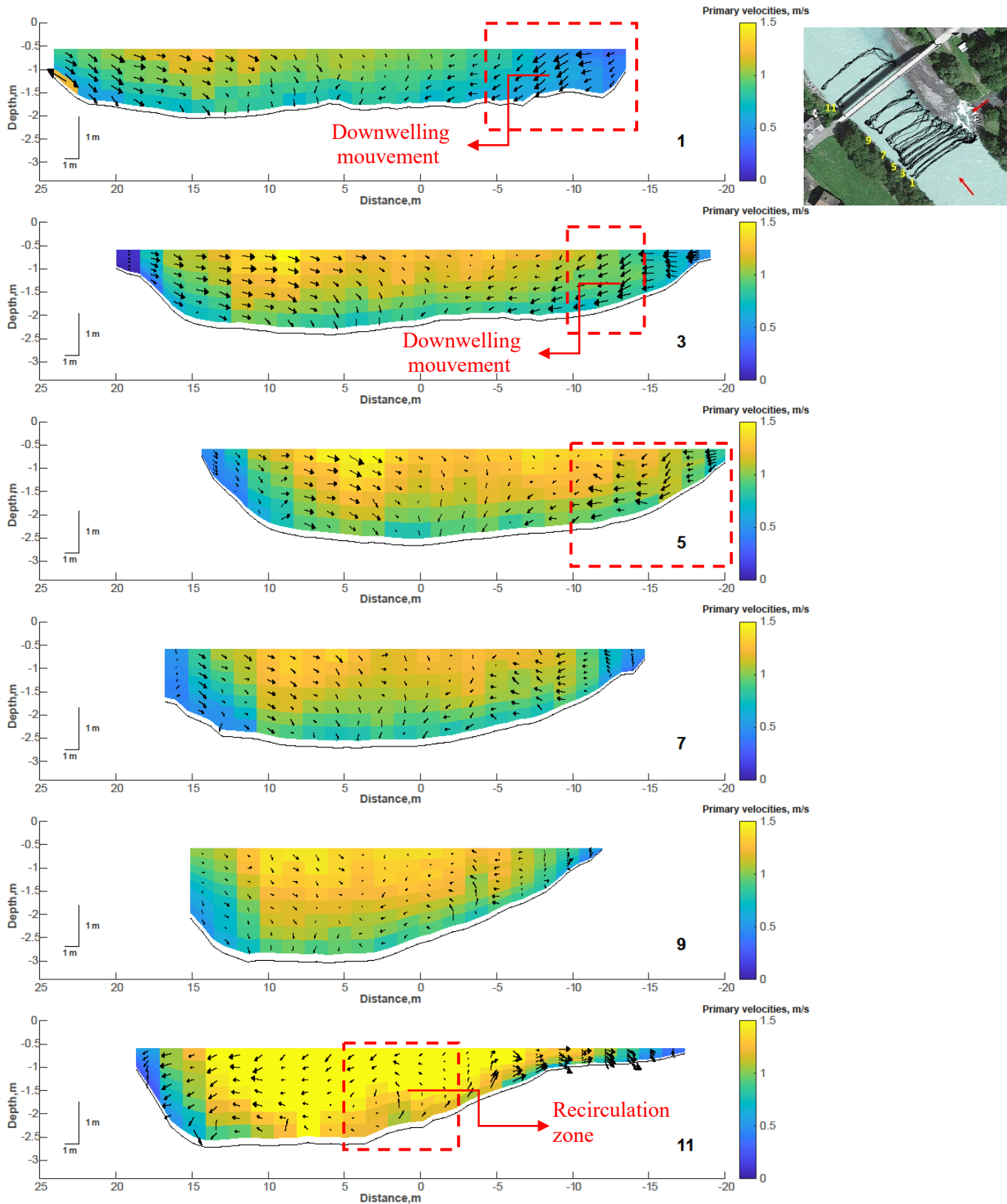
419

420 Figure 10. Grande Eau-Rhône confluence: patterns of morphological changes (a) and depth-
 421 averaged streamwise velocity vector distributions from moving ADCP measurement close to
 422 the free surface (b) and near the bed (c) and velocity magnitudes (contours in b & c)

423 3.2 Secondary flow velocities

424 Primary and secondary velocities were calculated for six cross sections at each
425 confluence (cross-section locations were added as small sketches to Figures 11-13). Figure 11
426 shows these results for selected cross sections of the Avançon-Rhône confluence. At cross
427 sections 1 and 3, flow originating from the tributary enters the main channel, with a
428 downwelling motion towards the bed and flow that is directed towards the main channel
429 throughout the flow depth (see the red boxes). At cross section 5 (see the red box), this flow
430 behaviour continues near the bed, but is reduced in magnitude near the surface. At section 7
431 there is what corresponds to the downstream junction corner with a zone of very low magnitude
432 velocity. To left of this zone, there is the continued presence of flow directed towards the true
433 left. This is also present at section 9, but by section 11 there is flow directed towards the true
434 right (Figure 11), at the downstream end of the bar (Figure 4a, Figure 8a).

435
436 These observations show clear tributary penetration into the main flow. However, this is
437 superimposed on a second large-scale flow structure. Sections 1 and 3 in particular (Figure 11),
438 also sections 5 and 7, show true right directed flow on the outer bank of the channel. When
439 combined with the tributary penetration, they result in flow convergence in the middle of each
440 section and downwelling, notably in Sections 1, 3 and 5. We attribute this to the channel
441 narrowing and flow acceleration, aided by the tributary mouth bar that forms at and downstream
442 of the Avançon. The downwelling seems to be displaced slightly to the true right side of the
443 deepest part of each section (i.e. the zone of scour) perhaps suggesting that the scour forms
444 during times when the tributary flow has a higher momentum and can penetrate more into the
445 main flow; but that it can be maintained at lower momentum ratios.

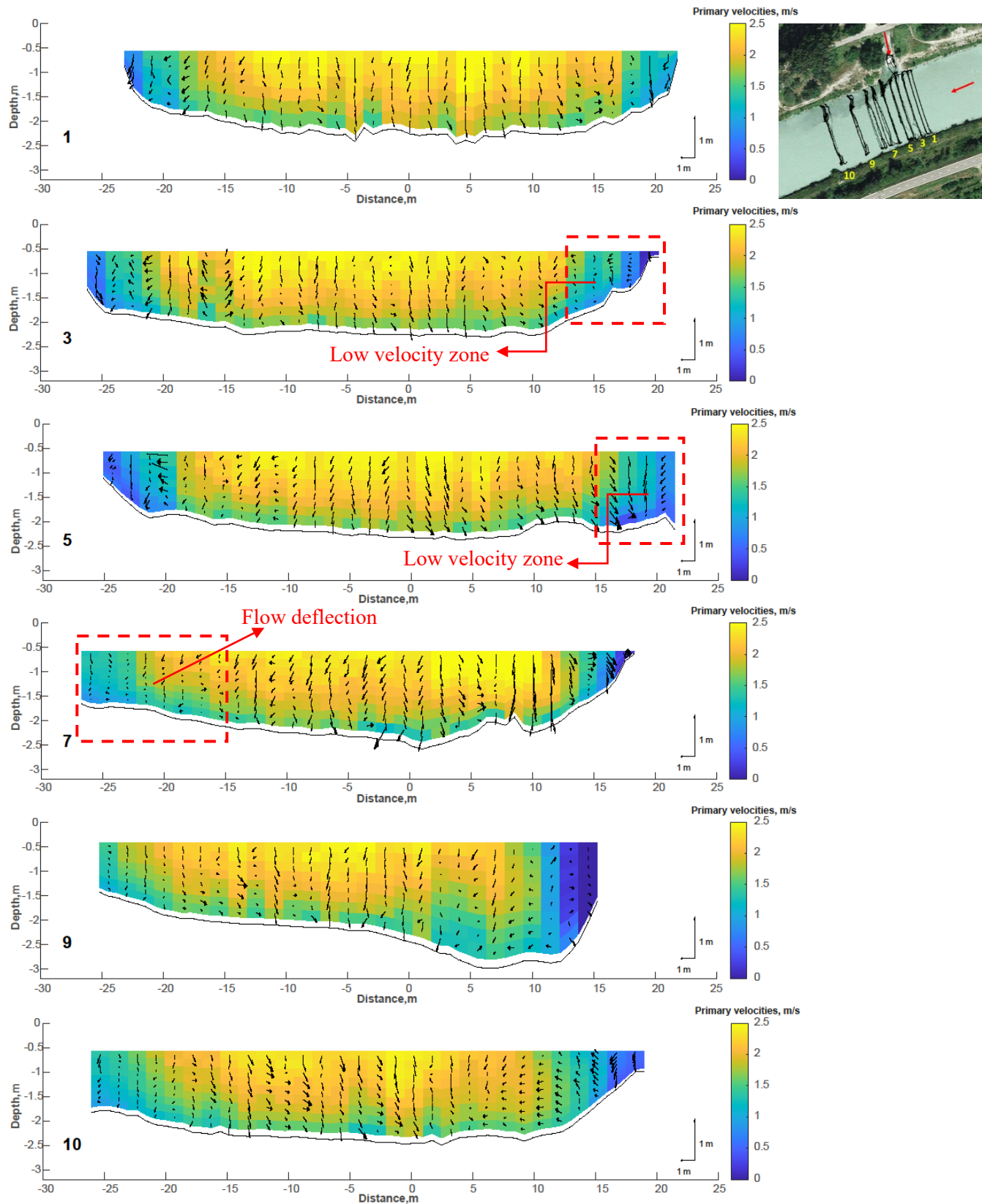


446
 447 Figure 11. Avançon-Rhône confluence: cross-section lines 1,3,5,7,9 and 11 with primary
 448 primary velocity contours (m/s) and secondary velocity vectors (m/s). Right parts of the figures
 449 represent the tributary side of the main channel. 0 datums in x axes are the middle point of the
 450 cross section and positive and negative values show the distance of the middle cross section
 451 point from each bank.

452 Figure 12 shows primary and secondary velocities for selected cross sections at the Lizerne-
453 Rhône confluence where the bed is concordant. Downstream of the junction apex, the flow
454 patterns differ significantly from those observed at the Avançon-Rhône confluence with a
455 discordant bed. The first thing that can be observed is that at cross-sections 3 and 5, the tributary
456 enters the main channel with a much lower magnitude of the penetration. Still, this penetration
457 is enough to push the mean Rhône flow toward the outer bank and to produce a large zone of
458 low flow on the tributary side of the main channel. By section 7, as this penetration is weak,
459 with the reduction of the flow curvature, the flow in the main channel reverses on the other side
460 of the tributary.

461
462 This suggests that whilst the momentum ratio at Lizerne-Rhône confluence is similar to that of
463 the Avançon-Rhône confluence, and both tributaries enter the main stem at 90 degrees, the
464 systematic flow convergence and divergence that is apparent in the Avançon-Rhône confluence
465 is not observed. The logical reason here could be the bed concordance at Lizerne-Rhône
466 confluence which disturbs the tributary flow over a greater depth and reduces its ability to
467 penetrate the main stem.

468
469 Finally, there are secondary motions in the main channel but these are less coherent and likely
470 to be a product of main channel turbulence anisotropy.

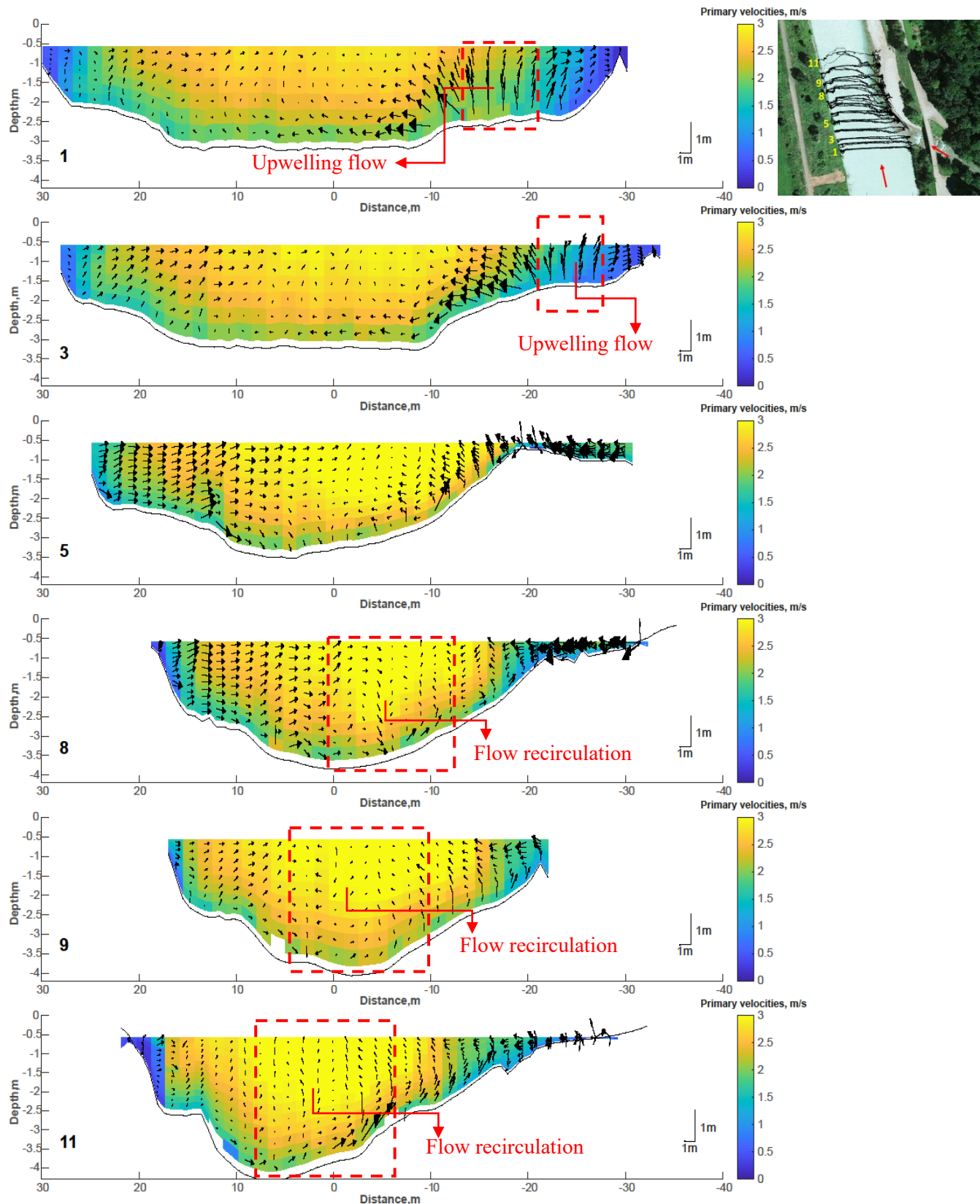


471

472 Figure 12. Lizerne-Rhône confluence: cross-section lines 1, 3,5,7,9 and 10 with primary
 473 velocity contours (m/s) and secondary velocity vectors (m/s). Right parts of the figures
 474 represent the inner bank. 0 datums in x axes are the middle point of the cross section and positive
 475 and negative values show the distance of the middle cross section point from each bank.

476 For the Grande Eau-Rhône confluence (Figure 13), for cross sections 1 and 3, there is very
477 strong upwelling where the tributary joins the Rhône, into very slow velocity zones upstream
478 and at the junction corner, which creates a small stagnation zone. Flow directed from the
479 tributary into the main flow is not really apparent, and this may reflect the much lower junction
480 angle. Tributary penetration is clear at section 5, the section that corresponds to the downstream
481 junction corner and this continues at section 8. By section 8, a very weak circulation cell has
482 developed (-14 to -20 m laterally), and this seems to be present at sections 9 and 11.

483
484 As with the Avançon, there is strong flow directed towards the true right on the outer bank of
485 the channel, from section 3 through to section 9, as the flow accelerates. The result is flow
486 convergence, with some evidence of flow convergence and downwelling at sections 5 and 8
487 (Figure 13). As with the Avançon, this downwelling is slightly displaced to the true right of the
488 scour hole. In this example, even though the tributary penetration seems to be reduced, the
489 presence of the bank attached tributary mouth bar seems to reduce channel width by almost
490 20%, causes flow acceleration and in turn causes the formation of channel scale secondary
491 circulation.



492

493 Figure 13. The Grande Eau-Rhône confluence: cross-section lines 1, 3,5,8,9 and 11
 494 with primary velocity contours (m/s) and secondary velocity vectors (m/s). Right parts of the figures
 495 represent the tributary side of the main channel. 0 datums in x axes are the middle point of the

496 cross section and positive and negative values show the distance of the middle cross section
497 point from each bank.

498 3.3 Angular momentum ratio

499 Table 1 included estimates of the angular momentum ratio for all three confluences.
500 That for the Avançon-Rhône confluence is the highest and would support penetration of the
501 tributary into the main channel being the highest as well. This value is lower for the Grande
502 Eau-Rhône confluence, despite the latter having a higher momentum ratio without correction
503 for angular effects, suggesting there should be less penetration of the Grande Eau into the
504 Rhône. For the Lizerne-Rhône confluence this value is the lowest which suggests there should
505 be a lower penetration of the tributary into the main stem. It might be expected that as angular
506 momentum increases, the likelihood of two-phase flow increases because it is more likely the
507 tributary has sufficient momentum to penetrate over the main channel flow. This is a hypothesis
508 that merits further evaluation, likely using numerical models.

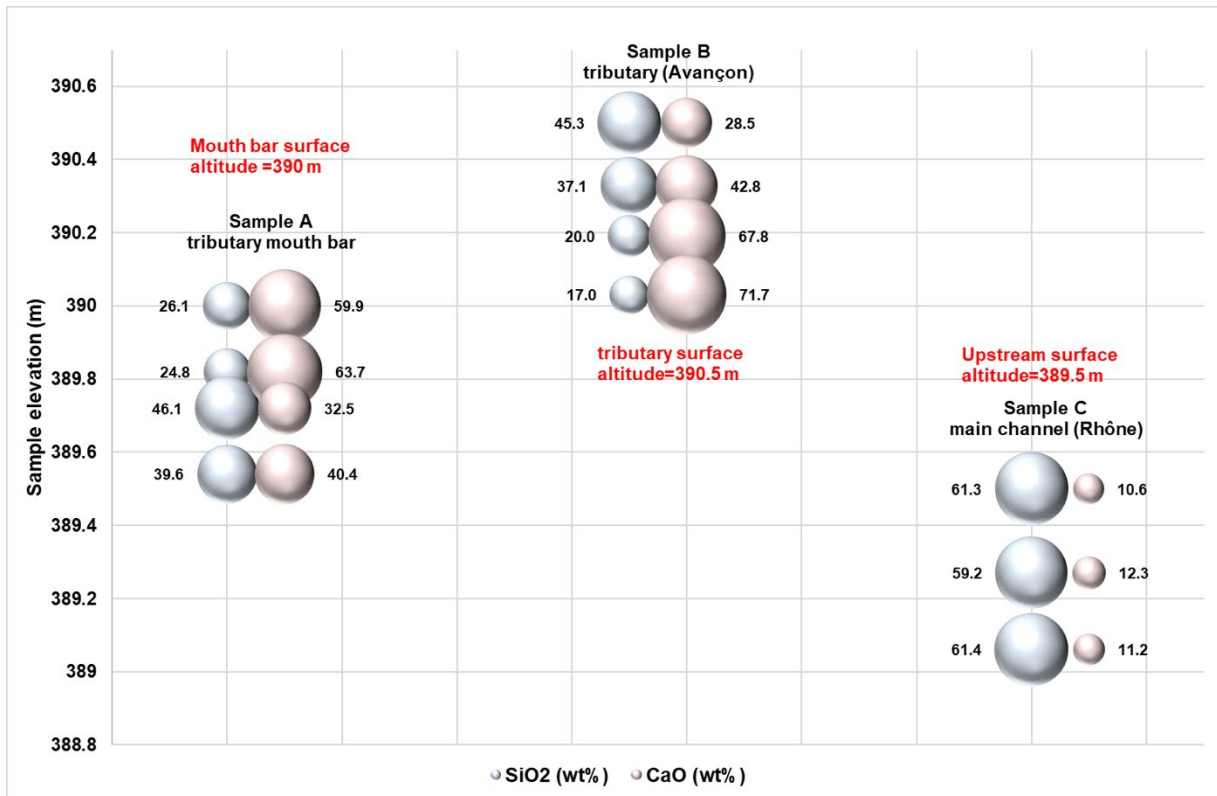
509 3.4 Tributary mouth bar mineralogy

510 Table 3 shows the validation of the provenance analyses. It confirms a good agreement
511 for the surface samples between the data of Stutenbacker et al. (2018) and the data used in this
512 study, perhaps less so for the proportion of CaO for the tributary sample in the Avançon. The
513 results also show that sediment in the Avançon tributary and in the Grande Eau surface samples
514 have elevated CaO and reduced SiO₂ as compared with the main Rhône such that we can use
515 the CaO and SiO₂ composition in the tributary mouth bar to indicate its likely provenance. We
516 were also able to access the Avançon tributary to do some samples at depth; this was not
517 possible in the Grande Eau due to the flow magnitude. The results are interesting as they show
518 that with depth the CaO concentration rises whilst the SiO₂ concentration falls, implying that
519 deeper in the tributary bed sediments the provenance becomes more typical of Helvetic. We
520 suggest that this reflects occasional penetration into the tributary of Rhône water and fine
521 sediment at particular low momentum ratios.
522

Site	This study: SiO ₂	This study: CaO	Stutenbacker et al. (2018) SiO ₂	Stutenbacker et al. (2018) CaO
Rhône upstream of Avançon (surface)	61.3%	10.6%	58.6%	12.2%
Rhône upstream of Avançon (0.23 m depth)	59.2%	12.3%	X	X
Rhône upstream of Avançon (0.44 m depth)	61.4%	11.2%	X	X
Avançon trib. (surface)	45.3%	28.5%	42.3%	37.8%
Avançon trib. (0.17 m depth)	37.1%	42.8%	X	X
Avançon trib. (0.26 m depth)	20.0%	67.8%	X	X
Avançon trib. (0.37 m depth)	17.0%	71.7%	X	X
Rhône upstream of Grande Eau (surface)	53.0%	15.1%	56.0%	11.0%
Grande Eau trib. (surface)	30.8%	30.3%	X	X

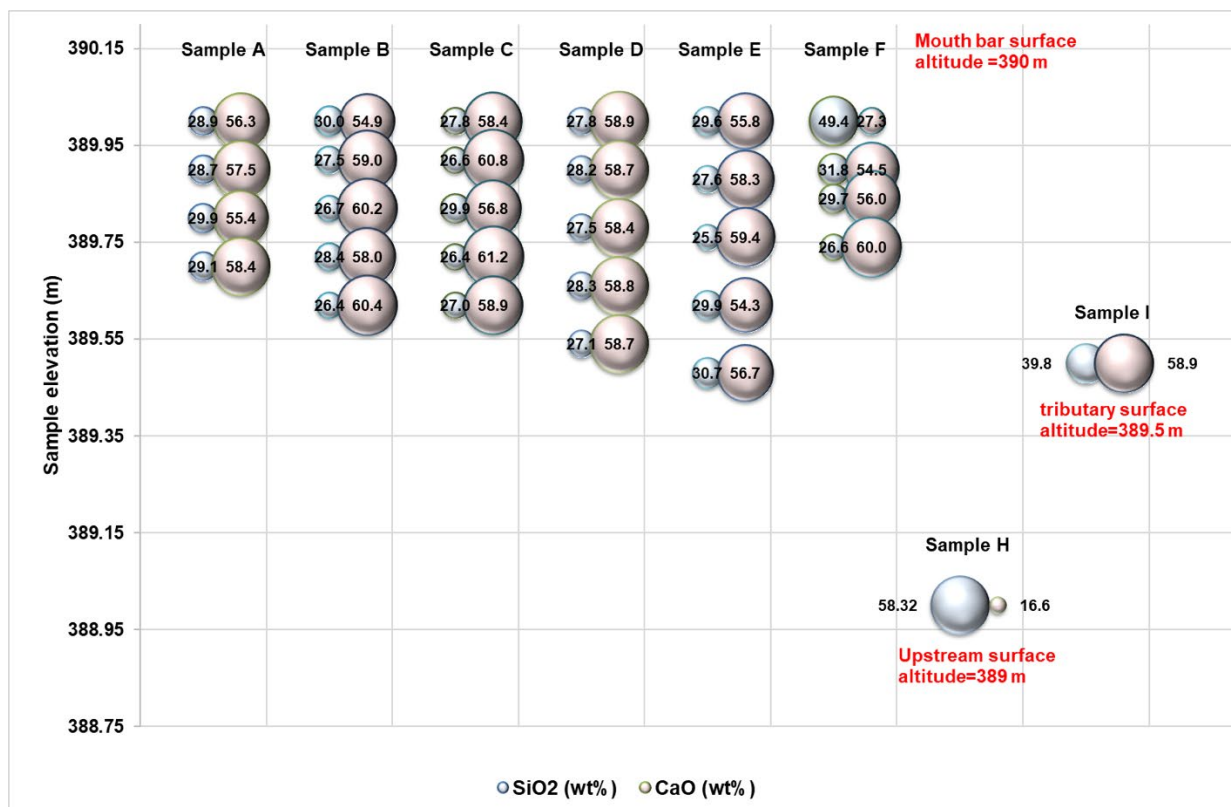
523
524 Table 3. Comparison of Stutenbacker et al. (2018) data (% by weight) with data acquired in this
525 study for sites upstream of the Avançon and Grande Eau junctions on the Rhône and in each
526 tributary.

527 Figure 14 shows data for the three locations sampled in the Avançon- Rhône confluence plotted
 528 against their absolute elevation. The sediment near the surface of the bar (sample A in Figure
 529 4a) has more CaO than SiO₂. There are two samples at comparable elevations to samples in the
 530 Avançon tributary. For both, proportions of bar and tributary samples are similar. However, the
 531 bottom two bar samples show much higher SiO₂ and lower CaO proportions, suggesting that
 532 lower in the bar, there is greater mixing in of sediment derived from the Rhône; the base of the
 533 bar is formed partly from main channel sediments.
 534



535
 536 Figure 14. Mineralogical provenance of the collected samples shown as proportional circles.
 537 Blue circles show the amount of SiO₂ and pink circles show the amount of CaO for the collected
 538 samples at Avançon-Rhône confluence

539 Samples in the Grande Eau-Rhône confluence are different. On the bar, samples (locations A-
 540 F in Figure 4c) contain only a modest amount of SiO₂, with almost all samples at all depths
 541 dominated by CaO (Figure 15). The tributary sediment (sample I) is also mostly CaO, whereas
 542 the main channel sediment (sample H) is mostly SiO₂. These data suggest that even at depth,
 543 sediment in the bar is mainly sourced from the Grande Eau. The junction angle is much smaller
 544 and it is probable that the Grande Eau can more readily steer its sediment into the zone of bar
 545 formation. It is possible that right at the most downstream sampled location there is some main
 546 channel sediment deposition (sample F), where a higher percentage of SiO₂ was observed near
 547 the surface, which could reflect finer sediment deposition of main channel derived sediment
 548 within the post-confluence zone. It is also possible that the fine sediments deposited at the
 549 downstream end of the bar are related to confluence hydrodynamics during bar formation in
 550 higher flow events. For instance, upwelling of fine sediment at the downstream end of the bar
 551 could be attributable to either: 1) the kinds of secondary circulation identified by Rhoads et al.
 552 (2009); or 2) to the development of a two-layer flow structure (Leite Ribeiro et al., 2012), where
 553 the flow from the main channel moves over the tributary flow and delivers sediment to the
 554 downstream end of the bar. We do not have data that could confirm either of these hypotheses.



555

556 Figure 15. Mineralogical provenance of the collected samples shown as proportional circles.
 557 Blue circles show amount of SiO₂ and pink circles show the amount of CaO for the collected
 558 samples at Grande Eau-Rhône confluence

559 **4 Discussion**

560 The results of this study reveal the complex flow behaviour and morphological changes in three
 561 confluences with very low momentum ratios during measurement but very different junction
 562 angles and long-term rates of sediment supply. In this section we discuss the similarities and
 563 differences in flow structure and morphological aspects of these three confluences as compared
 564 to previous conceptual models of river channels with different characteristics, proposed by Best
 565 (1987,1988), Mosely (1976) and Leite Ribeiro et al. (2012). Overall, the general flow and
 566 morphological patterns are highly influenced by the junction angle and sediment supply.

567 **4.1 Sediment transport rate**

568 As there was no sediment transport in the tributary during measurement, transport rates
 569 for tributary sediment transporting events were not estimated because sediment transport
 570 capacity calculations suggest errors across 5 orders of magnitude for this kind of river
 571 (Antoniazza et al., 2022) but also because sediment transport is strongly influenced by changes
 572 in sediment supply. Comparison of two case studies with different tributary sourced sediment
 573 supply (Avançon-Rhône confluence and Lizerne-Rhône confluence) suggests that if the
 574 tributary is able to supply significant sediment supply (as at the Avançon-Rhône confluence)
 575 the formation of a pronounced bed discordance and tributary mouth bar is possible. The effect
 576 of bed discordance on flow dynamics and bed morphology has been reported by Biron et al.
 577 (1996a, 1996b), Best and Rhoads (2008), Djordjevic (2008) and Leite Ribeiro et al. (2012).
 578 Leite Ribeiro et al. (2012) were the first to draw attention to the potentially modifying effect of
 579 tributary sediment delivery, by studying the junction morphology that formed where the
 580 tributary had a low flow momentum compared to the main channel.
 581

582 In the experiments of Leite Ribeiro et al. (2012) and Guillén Ludena et al. (2015, 2016), the
583 discharge in the tributary and the main stem were applied to sediment transport formulae to set
584 sediment supply rates. Their experiments were performed in the laboratory with a constant
585 sediment discharge, which was supplied to the tributary and the main channel. They also
586 discussed the formation of the two-layer flow associated with the bed discordance. In field
587 cases, it is likely that the tributary supplies sediment at different times (and with different
588 calibre) to the main channel because of different distances between the confluence and potential
589 sediment sources and different hydrological regimes.

590
591 In low momentum ratio river confluences, if the sediment supply from the tributary is high
592 enough, the low momentum does not result in particularly strong jet formation (Figure 11) and
593 the tributary flow seems to be rapidly-steered, even at the surface (Figure 8). However, it is
594 clear that the tributary mouth bar extends downstream from the downstream junction corner
595 (Figure 8) with a sustained narrowing of the main channel and flow acceleration (Figure 8).
596 There is the appearance of a scour hole, flow convergence and some flow downwelling (Figure
597 11). This is likely to reflect the combined effects of tributary penetration and bar driven main
598 channel narrowing. A slight displacement of the downwelling to the tributary side of the scour
599 hole suggests that the scour hole may have formed when the tributary momentum was higher,
600 which would increase flow acceleration, downwelling and hence erosion. The tributary mouth-
601 bar that extends along the inner bank of the main channel is related either to the low flow
602 velocity zone or to the flow recirculation zone, which favour sediment deposition therein. Most
603 of the sediment that form this bar could be a result of the sediment deposition sourced from the
604 tributary.

605
606 Biron et al. (1993) discussed the absence of marked scour holes at discordant confluences.
607 Guillén Ludeña et al., (2015) observed a deeper scour hole at the outer bank of the main channel
608 and a narrower and higher bank-attached bar at the inner bank as discussed above. It is likely
609 that these differences relate to tributary sediment supply differences. These differences could
610 also be related to the confluence configuration for each case; rigid lateral banks in the case of
611 Guillen-Ludeña et al. (2015); and erodible banks in the case of Biron et al. (1993). The
612 discharge ratio may also play a role in these differences. Where tributary sediment supply is
613 higher and a tributary mouth bar can form and attach itself to the bank downstream of the
614 tributary, channel cross-section area is reduced, flow is accelerated and converges, and the
615 combined flow acceleration and downwelling flow which could be the result of either secondary
616 circulation or bed discordance (there is no data available for this study to confirm the
617 mechanism). Intriguingly, the sediment provenance studies suggest that the tributary mouth bar
618 relates to sediment sourced from both the tributary and the main channel because the sediments
619 originating from the main channel may have been transported there by flow upwelling or by
620 secondary currents (Rhoads, 2009). Observations suggest that tributary mouth bars can be
621 periodically trimmed and eroded by the main channel, to leave a more classical discordant
622 confluence (Moesly, 1976), with weaker tributary mouth bar penetration, more typical of what
623 was observed by Biron et al. (1993). In such situations, as sediment supply in the main channel
624 or the tributary increases, sediment from the main channel is likely to move underneath the
625 tributary explaining why more Rhône sediment than expected was found at the base of the
626 Avançon tributary mouth bar; the sediments originating from the main channel may have been
627 transported there by flow upwelling or by secondary currents (Rhoads, 2009). Further fieldwork
628 or computational modelling is needed to assess this effect.

629
630 On the other hand, if the tributary sediment supply is not significant (Lizerne-Rhône
631 confluence), the bed is concordant. For the same momentum ratio, this reduces tributary
632 penetration. A weak mixing interface moves toward the inner bank farther downstream and

633 prevents the formation of the downstream attached bar at this bank, even with sediment
634 provided by the main river, in the absence of tributary sediment supply. There is perhaps some
635 evidence of scour in this zone, attached to the tributary side of the channel (Figure 9).

636
637 Comparing the Avançon confluence and the Lizerne confluence, which have the same junction
638 angle and very similar momentum ratios at the time of measurement, but very different
639 sediment supply rates, it is apparent that markedly different bathymetries and flow structures
640 form. In forming a tributary mouth bar that may then become attached to the downstream true
641 inner bank, tributary sourced sediment can lead to substantial impacts on the main channel flow,
642 even at very low flow momentum ratios and when the tributary is no longer actively supplying
643 sediment. This is a legacy effect with the bar forming at times when the tributary momentum is
644 likely to have been higher (i.e. when it is capable of delivering sediment) and that lasts as long
645 as the main channel is unable to erode the bar that forms.

646 4.2 Junction angle and angular momentum ratio

647 The junction angle controls the curvature of merging flows, and the comparison of the
648 Avançon (higher junction angle) and Grande Eau (lower junction angle) suggest that lower
649 junction angle but high tributary sediment supply will modify bathymetry in degree rather than
650 in kind. Previous laboratory and field studies have shown that increasing the junction angle
651 enhances the curvature of the merging flow and facilitates the penetration of the tributary flow
652 into the main channel (Best, 1988; Rhoads & Kenworthy, 1995; Rhoads & Sukhodolov, 2001).
653 Our results support these conclusions, in that the Avançon (with higher junction angle)
654 penetrated into the Rhone more than the Grande Eau (with lower junction angle); and this effect
655 was captured by correcting the momentum ratios for angular effects. Both confluences have
656 discordance and were measured at similar momentum ratios, and so the formation of a relatively
657 weak jet-like tributary flow at the Avançon is likely to be a result of a greater junction angle.
658 This is the classic two-layer flow proposed by Leite Ribeiro et al. (2012). This two-layer flow
659 was not observed at the Grande Eau, possibly because of a lower junction angle which leads to
660 a lower angular momentum ratio and thus less penetration of tributary flow into the main
661 channel. One might expect a greater likelihood for two-layer flow as angular momentum ratio
662 increases because the tributary will have greater momentum to penetrate over the main channel
663 flow. This hypothesis could be assessed in future work, perhaps with the aid of numerical
664 modelling. On the other hand, although difficult to detect conclusively in the data, a zone of
665 stagnation was found at Grande Eau upstream of the junction throughout the flow depth, and a
666 stagnation is more likely to occur if there is two-layer flow because the penetrating tributary
667 flow creates a barrier.

668
669 Given that both the Avançon and Grande Eau delivered sediment to the Rhone, our results allow
670 evaluation of the influence of junction angle for tributaries with sediment supply. Junction angle
671 appears to modify the effects of tributary sediment delivery. The tributary mouth bar that
672 formed at the Grande Eau contained less main river sediment and was dominated by sediment
673 supplied from the tributary. The reduced junction angle at the Grande Eau appears to have
674 facilitated the re-orientation of tributary supplied coarse sediment, forming the downstream
675 attached bar, with tributary supplied sediment throughout its depth. This is field confirmation
676 of the laboratory observations of Guillén-Ludeña et al (2016). The bed discordance at the
677 Avançon-Rhône confluence and a higher junction angle lead to a greater penetration of the
678 tributary into the main channel. It may also encourage formation of a larger recirculation zone
679 downstream of the junction, which perhaps allows main channel sediment to recirculate onto
680 the bar, particularly during conditions of low tributary flow. That could be the reason why the
681 mouth bar is formed with both tributary and mainstream sediment.

682 4.3 Hydrodynamics

683 Mosley (1976) and Best (1987, 1988) showed that at momentum ratios close to one and
684 for channels that both turn through the same angle, two helical cells form downstream of the
685 junction, close to the confluence, within the near-field region defined as the confluence
686 hydrodynamic zone (e.g. Konsoer and Rhoads, 2014). Mosley (1976) showed that where the
687 momentum ratio is near one, these helical cells are well-developed counter-rotating and occupy
688 equal proportions of the main channel cross section. By increasing the momentum ratio, the
689 tributary adjacent cell starts to prevail and occupies a greater proportion of the channel cross-
690 section. Mosley also showed that for momentum ratios less than one, the penetration of the flow
691 originating from the tributary into the main channel reduces (see also Rhoads and Johnson,
692 2018) and the position of the mixing interface migrates towards the tributary. With very low M_r
693 (e.g. Riley and Rhoads (2012) report data for $M_r=0.27$) there may be no tributary side secondary
694 circulation cell. Results obtained for Lizerne-Rhône confluence are in good agreement with
695 these previous findings. For both the Avançon and the Grande-Eau confluences, significant
696 secondary circulation was found even at very low momentum ratios, and it is logical to conclude
697 that what makes these cases different to the more general model is the presence of high rates of
698 coarse sediment supply and tributary mouth bar formation and discordance, expected for
699 tributaries draining mountain zones. Such effects are likely to be modified by junction angle.
700 In turn, this finding suggests that momentum ratio on its own cannot be used to generalise the
701 morphodynamics of confluences: how the momentum is distributed with respect to the main
702 channel (i.e. a discordance index) as well as modification of the momentum ratio to become an
703 angular momentum ratio is needed.

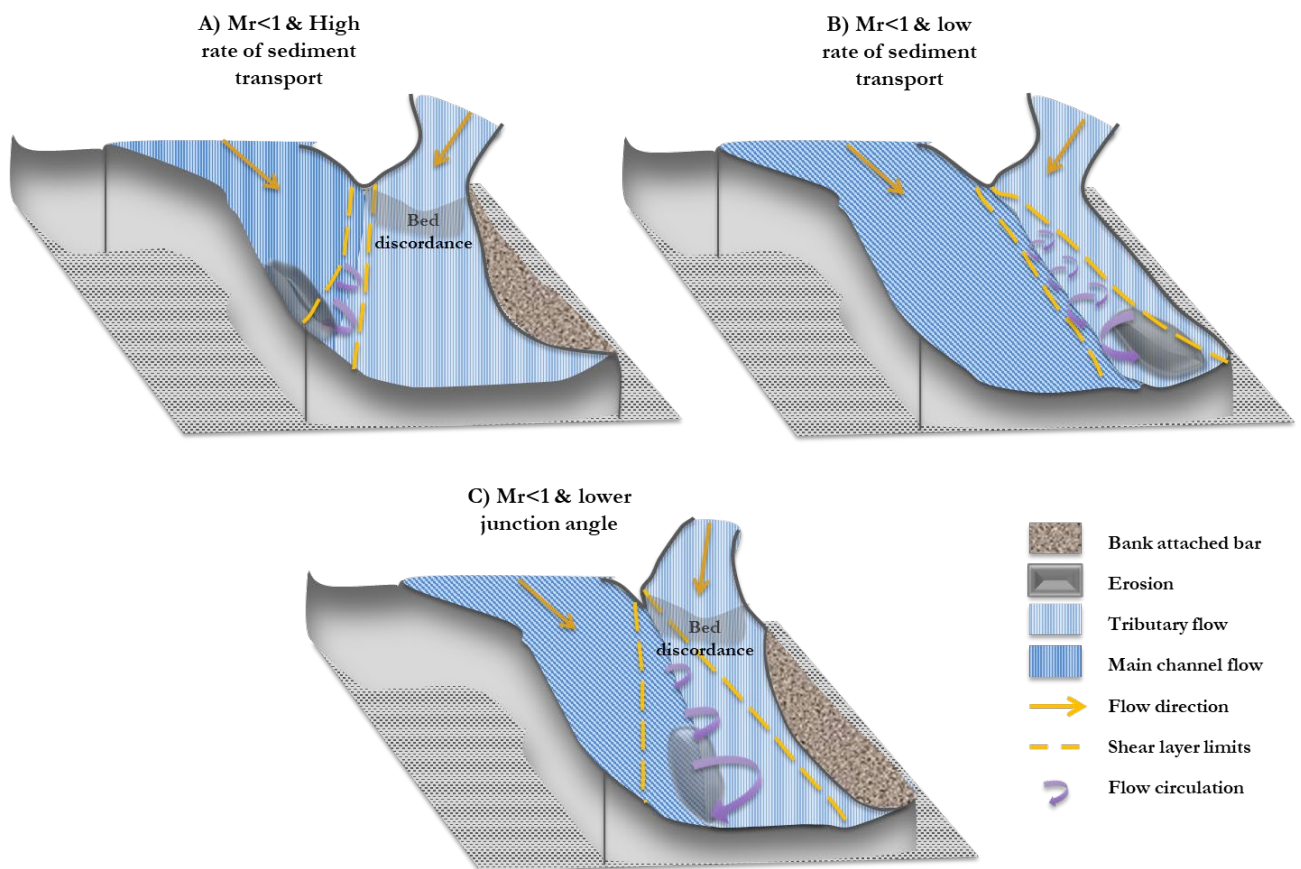
704
705 It is the tributary with the lowest angular momentum that is likely to penetrate least into the
706 confluence. This may reduce to below one for the momentum ratio at which both the main stem
707 and tributary have a significant influence on the confluence flow field. As the momentum ratio
708 falls further, the tributary influence should progressively decline. It then may be necessary to
709 have angular momentum ratios for both the concordant and the discordant case to capture
710 tributary sediment delivery effects.

711 4.4 Conceptual Model for Low Momentum Ratio Confluences

712 The evidence obtained from this study shows that none of the existing conceptual
713 models can fully explain the flow behaviour in confluences with low momentum ratio.
714 Although Boyer et al., (2006) has reported conceptual models for $M_r < 1$, their conceptual model
715 is limited to high flow conditions where there is the presence of bed discordance. They also
716 reported the absence of the scour hole at the outer bank. Leite Ribeiro et al., (2012) and Guillén
717 Ludeña et al., (2015, 2016, 2017) studied river confluences with low momentum ratio, however
718 their models were limited to a specific case of river confluences with high and equivalent rates
719 of sediment delivery from the tributary and the main channel. Their studies also were limited
720 to discordant confluences with large junction angles. Best (1988) investigated asymmetric
721 confluences with concordant beds, in a small laboratory flume and Leite Ribeiro et al., (2012)
722 showed important differences between this conceptual model and confluences with low
723 momentum ratio and high rates of sediment delivery, such as found in mountainous regions.

724
725 With regard to the above discussion, Figure 16 shows a proposed conceptual framework for
726 river confluences characterized with very low momentum ratio and various rates of sediment
727 supply from the tributary into the main channel. As shown in Figure 16A, in the presence of a
728 significant discordance at the mouth of the tributary, due to the high sediment supply originating
729 from the tributary, the scour hole is shifted from the confluence zone toward the outer bank.
730 High tributary sediment supply forms a mouth bar and this may extend downstream attached to
731 the tributary side of the bank. This bar may develop from deposition of main channel sediment

732 as well as tributary sediment. There is no evidence for the active sediment transport in this case
 733 because the tributary flow is not competent enough to supply a high amount of sediment all the
 734 time, but in high sediment transport periods, due to the presence of the two layer flow which
 735 results in the formation of the secondary circulation, sediment from the main channel could
 736 move under that of the tributary and the bar could be vertically developed by the deposition of
 737 the tributary sediment. Decreasing the junction angle (Figure 16C) means the reduction of the
 738 angular momentum ratio and the penetration of the tributary flow into the main channel; results
 739 in a scour hole more towards the middle of the main channel; and is associated with a bar along
 740 the tributary side bank of the main channel, downstream of the confluence. This bar develops
 741 due to deposition of primarily tributary sediment because the tributary is better able to steer the
 742 sediment to orient itself parallel to the main flow and develop the bar more laterally than the
 743 Avançon confluence. In the case where the sediment transported from the tributary into the
 744 main channel is not significant or the dominant sediment supply originates from the main
 745 channel (Figure 16B), no bed discordance develops, the scour occurs near the inner bank, and
 746 the formation of the mouth bar is absent.



747
 748 Figure 16. Proposed conceptual model for A) $Mr < 1$ and high rate of sediment transport, B)
 749 $Mr < 1$ and low rate of sediment transport and C) $Mr < 1$ and high rate of sediment transport and
 750 lower junction angle (Boyer et al. 2006)

751 5 Conclusion

752 The present study based on field data at three medium sized confluences with low momentum
 753 ratio show that the tributaries which carry a significant amount of sediment into the main
 754 channel, have hydrodynamics and morphodynamics patterns which differ from classical
 755 models. They are often associated with a discordant bed. A downstream attached bar and a
 756 pronounced scour hole can also be observed, the latter reflecting the effects of bar formation on
 757 channel capacity and flow acceleration, convergence and downwelling. The result is that even
 758 at very low momentum ratios it is possible to have significant secondary circulation in the main

759 channel due to the legacy of previously delivered and deposited sediment as a tributary mouth
760 bar.

761 Results indicate that the downstream bar can have different sediment origins, according to the
762 angle of the junction. If the junction angle is lower, this bar can be a result of the tributary
763 sediment supply. By increasing the junction angle, as the curvature of the merging flow is also
764 increased, a jet may form, allowing main channel sediment to penetrate under the tributary
765 inflow and accumulate at the base of the bar, as was measured in this study.

766
767 The results of the present study also demonstrate that at low momentum ratio confluences where
768 the tributary supplies less sediment into the main channel, the tributary mouth bar does not form
769 and it is even possible for a scour hole to form where a bar would be deposited in situations
770 where the tributary delivers sediment. We attribute this to the reduced penetration of the
771 tributary, leaving mixing closer to the tributary side of the channel.

772
773 As the results of the present study are limited to a small range of confluences with low
774 momentum ratio and specific confluence configurations, further work is needed to determine
775 how variations in other factors controlling flow pattern at confluences, such as the discharge
776 ratio, junction angle, confluence planform symmetry, and variations in sediment transport rate,
777 interact with hydrodynamics and morphodynamics of mountain river confluences. What this
778 study has shown is that the sediment transport rate, discordance and angular momentum should
779 be considered when defining the low momentum ratio river confluences and evaluating
780 confluence hydrodynamics and morphodynamics.

781

782 **Acknowledgements**

783 The work was supported by Swiss National Science Foundation Grant 200021_160020. The
784 data have been uploaded and archived in a PANGAEA repository at
785 <https://issues.pangaea.de/browse/PDI-21636>.

786 **References**

- 787 Ashmore, P., Parker, G., 1983. Confluence scour in coarse braided streams. *Water Resour. Res.*
788 19, 392–402.
- 789 Ashmore, P.E., Ferguson, R.I., Prestegard, K.L., Ashworth, P.J., Paola, C., 1992. Secondary
790 flow in anabranch confluences of a braided, gravel-bed stream. *EARTH Surf. Process.*
791 *LANDFORMS* 17, 299–311.
- 792 Antoniazza G., Nicollier T., Boss S., Mettra F., Badoux A., Schaepli B., Rickenmann D., Lane
793 S. N., 2022. Hydrological drivers of bedload transport in an Alpine watershed. *Water*
794 *Resources Research*. Peer-reviewed.
- 795 Best, J.L., 1987. Flow dynamics at river channel confluences: Implications for sediment
796 transport and bed morphology. *Recent Dev. Fluv. Sedimentol. Spec. Publ. SEPM Soc.*
797 *Sediment. Geol.* 27–35. <https://doi.org/10.2110/pec.87.39.0027>
- 798 Best, J.L., 1988. Sediment transport and bed morphology at river channel confluences.
799 *Sedimentology* 35, 481–498. <https://doi.org/10.1111/j.1365-3091.1988.tb00999.x>
- 800 Biron, P., Best, J.L., Roy, A.G., 1996a. Effects of Bed Discordance on Flow Dynamics at Open
801 Channel Confluences. *J. Hydraul. Eng.* 122, 676–682.
802 [https://doi.org/10.1061/\(ASCE\)0733-9429\(1996\)122:12\(676\)](https://doi.org/10.1061/(ASCE)0733-9429(1996)122:12(676))
- 803 Biron, P.M., Roy, A.G., Best, J.L., 1996b. Turbulent flow structure at concordant and
804 discordant open-channel confluences. *Exp. Fluids* 21, 437–446.
805 <https://doi.org/10.1007/BF00189046>
- 806 Boyer, C., Roy, A.G., Best, J.L., 2006. Dynamics of a river channel confluence with discordant
807 beds: Flow turbulence, bed load sediment transport, and bed morphology. *J. Geophys.*
808 *Res. Earth Surf.* 111, 1–22. <https://doi.org/10.1029/2005JF000458>
- 809 Bradbrook, K.F., Lane, S.N., Richards, K.S., Biron, P.M., Roy, A.G., 2001. Role of Bed
810 Discordance at Asymmetrical River Confluences. *J. Hydraul. Eng.*
811 [https://doi.org/10.1061/\(ASCE\)0733-9429\(2001\)127:5\(351\)](https://doi.org/10.1061/(ASCE)0733-9429(2001)127:5(351))
- 812 De Serres, B., Roy, A.G., Biron, P.M., Best, J.L., 1999. Three-dimensional structure of flow at
813 a confluence of river channels with discordant beds. *Geomorphology* 26, 313–335.
814 [https://doi.org/10.1016/S0169-555X\(98\)00064-6](https://doi.org/10.1016/S0169-555X(98)00064-6)
- 815 Dietrich, W. E., and Smith, J. D., 1983. Influence of the point bar on flow through curved
816 channels, *Water Resources Research*, 19, 1173– 1192. [http://doi.org/](http://doi.org/10.1029/WR019i005p01173)
817 [10.1029/WR019i005p01173](http://doi.org/10.1029/WR019i005p01173)
- 818 Dinehart, R.L., Burau, J.R., 2005. Averaged indicators of secondary flow in repeated acoustic
819 Doppler current profiler crossings of bends. *Water Resour. Res.* 41, 1–18.
820 <https://doi.org/10.1029/2005WR004050>
- 821 Djordjevic, D. Numerical study of 3D flow at right-angled confluences with and without
822 upstream planform curvature. *J. Hydroinform.* 2013, 15, 1073–1088.

- 823 Gartner, J.W., 2004. Estimating suspended solids concentrations from backscatter intensity
824 measured by acoustic Doppler current profiler in San Francisco Bay, California. *Mar.*
825 *Geol.* 211, 169–187. <https://doi.org/10.1016/j.margeo.2004.07.001>
- 826 Guillén-Ludeña, S., 2015. Hydro-morphodynamics of open-channel confluences with low
827 discharge ratio and dominant tributary sediment supply. *Ec. Polytech. Fédérale*
828 *Lausanne, Switz.* 6716. <https://doi.org/10.5075/epfl-thesis-6716>
- 829 Guillén-Ludeña, S., Franca, M.J., Cardoso, A.H., Schleiss, A.J., 2015. Hydro-morphodynamic
830 evolution in a 90° movable bed discordant confluence with low discharge ratio. *Earth*
831 *Surf. Process. Landforms* 40, 1927–1938. <https://doi.org/10.1002/esp.3770>
- 832 Guillén-Ludeña, S., Franca, M.J., Cardoso, A.H., Schleiss, A.J., 2016. Evolution of the
833 hydromorphodynamics of mountain river confluences for varying discharge ratios and
834 junction angles. *Geomorphology* 255, 1–15.
835 <https://doi.org/10.1016/j.geomorph.2015.12.006>
- 836 Guillén Ludeña, S., Cheng, Z., Constantinescu, G., Franca, M.J., 2017. Hydrodynamics of
837 mountain-river confluences and its relationship to sediment transport. *J. Geophys. Res.*
838 *Earth Surf.* 122, 901–924. <https://doi.org/10.1002/2016JF004122>
- 839 Gunawan, B., Sterling, M., Knight, D.W., 2010. Using an acoustic Doppler current profiler in
840 a small river. *Water Environ. J.* 24, 147–158. <https://doi.org/10.1111/j.1747-6593.2009.00170.x>
- 842 Hauet, A., Muste, M., H-C., H., 2009. High spatial resolution data acquisition for the
843 geosciences: kite aerial photography. *Earth Surf. Process. Landforms* 34, 242–252.
844 <https://doi.org/10.1002/esp>
- 845 Kostaschuk, R., Best, J., Villard, P., Peakall, J., Franklin, M., 2005. Measuring flow velocity
846 and sediment transport with an acoustic Doppler current profiler. *Geomorphology* 68,
847 25–37. <https://doi.org/10.1016/j.geomorph.2004.07.012>
- 848 Kenworthy, S.T., Rhoads, B.L., 1995. Hydrologic control of spatial patterns of suspended
849 sediment concentration at a stream confluence. *J. Hydrol.* 168, 251–263.
850 [https://doi.org/10.1016/0022-1694\(94\)02644-Q](https://doi.org/10.1016/0022-1694(94)02644-Q)
- 851 Konsoer, K.M., Rhoads, B.L., 2014. Spatial–temporal structure of mixing interface turbulence
852 at two large river confluences. *Environ. Fluid Mech.* 14, 1043–1070.
853 <https://doi.org/10.1007/s10652-013-9304-5>
- 854 Lane, S.N., Parsons, D.R., Best, J.L., Orfeo, O., Kostaschuk, R. a., Hardy, R.J., 2008. Causes
855 of rapid mixing at a junction of two large rivers: Río Paraná and Río Paraguay,
856 Argentina. *J. Geophys. Res. Earth Surf.* 113, 1–16.
857 <https://doi.org/10.1029/2006JF000745>
- 858 Leite Ribeiro, M., 2011. Influence of Tributary Widening on Confluence Morphodynamics. *Ec.*
859 *Polytech. Fédérale Lausanne, Lausanne, Switz.* <https://doi.org/10.5075/epfl-thesis-4951>
- 860 Leite Ribeiro, M., Blanckaert, K., Roy, A.G., Schleiss, A.J., 2012. Flow and sediment dynamics
861 in channel confluences. *J. Geophys. Res. Earth Surf.* 117.
862 <https://doi.org/10.1029/2011JF002171>

- 863 Lewis, Q.W., Rhoads, B.L., 2015. Rates and patterns of thermal mixing at a small stream
864 confluence under variable incoming flow conditions. *Hydrol. Process.* 29, 4442–4456.
865 <https://doi.org/10.1002/hyp.10496>
- 866 Li, K., Yuan, S., Tang, H., Xiao, Y., Xu, L., Huang, S., Rennie, C.D., Gualtieri, C.A. Field study
867 of near-junction-apex flow at a large river confluence and its response to the effects of
868 floodplain flow. *J. Hydrology*, 610:127983,2022.
- 869 Moradi, G., Vermeulen, B., Rennie, C.D., Cardot, R., Lane, S.N., 2019. Evaluation of aDcp
870 processing options for secondary flow identification at river junctions. *Earth Surf.*
871 *Process. Landforms.* <https://doi.org/10.1002/esp.4719>
- 872 Mosley, M.P., 1976. An Experimental Study of Channel Confluences. *J. Geol.*
873 <https://doi.org/10.1086/628230>
- 874 Parsons, D.R., Best, J.L., Orfeo, O., Hardy, R.J., Kostaschuk, R., Lane, S.N., 2005. Morphology
875 and flow fields of three-dimensional dunes, Rio Paraná, Argentina: Results from
876 simultaneous multibeam echo sounding and acoustic Doppler current profiling. *J.*
877 *Geophys. Res. Earth Surf.* 110, 1–9. <https://doi.org/10.1029/2004JF000231>
- 878 Petrie, J., Diplas, P., Nam, S., Gutierrez, M.S., 2010. Local boundary shear stress estimates
879 from velocity profiles measured with an ADCP. *River Flow 1749–1755.*
- 880 Rennie, C.D., Villard, P.V., 2004. Site specificity of bed load measurement using an acoustic
881 Doppler current profiler. *J. Geophys. Res.* 109, 1–15.
882 <https://doi.org/10.1029/2003jf000106>
- 883 Rennie, C.D., Millar, R.G., 2004. Measurement of the spatial distribution of fluvial bedload
884 transport velocity in both sand and gravel. *Earth Surf. Process. Landforms* 29, 1173–
885 1193. <https://doi.org/10.1002/esp.1074>
- 886 Rennie, C. D., Church, M., 2010. Mapping spatial distributions and uncertainty of water and
887 sediment flux in a large gravel bed river reach using an acoustic Doppler current profiler,
888 *J. Geophys. Res.*, 115, F03035. <https://doi.org/10.1029/2009JF001556>.
- 889 Rhoads, B.L., Kenworthy, S.T., 1995. Flow structure at an asymmetrical stream confluence.
890 *Geomorphology* 11, 273–293. [https://doi.org/10.1016/0169-555X\(94\)00069-4](https://doi.org/10.1016/0169-555X(94)00069-4)
- 891 Rhoads, B.L., Sukhodolov, N., 2001. Field investigation of three-dimensional flow structure.
892 *Water Resour. Res.* 37, 2393–2410. <https://doi.org/10.1029/2001WR000316>
- 893 Rhoads, B.L., Sukhodolov, A.N., 2008. Lateral momentum flux and the spatial evolution of
894 flow within a confluence mixing interface. *Water Resour. Res.* 44, 1–17.
895 <https://doi.org/10.1029/2007WR006634>
- 896 Rhoads, B.L., Riley, J.D., Mayer, D.R., 2009. Response of bed morphology and bed material
897 texture to hydrological conditions at an asymmetrical stream confluence.
898 *Geomorphology* 109, 161–173. <https://doi.org/10.1016/j.geomorph.2009.02.029>
- 899 Rhoads, B.L., Johnson, K.K., 2018. Three-dimensional flow structure, morphodynamics,
900 suspended sediment, and thermal mixing at an asymmetrical river confluence of a
901 straight tributary and curving main channel. *Geomorphology* 323, 51–69.
902 <https://doi.org/10.1016/j.geomorph.2018.09.009>

- 903 Riley, J.D., Rhoads, B.L., 2012. Flow structure and channel morphology at a natural confluence
904 meander bend. *Geomorphology* 163–164, 84–98.
905 <https://doi.org/10.1016/j.geomorph.2011.06.011>
- 906 Riley, J.D., Rhoads, B.L., Parsons, D.R., Johnson, K.K., 2015. Influence of junction angle on
907 three-dimensional flow structure and bed morphology at confluence meander bends
908 during different hydrological conditions. *EARTH Surf. Process. LANDFORMS* 40,
909 252–271. <https://doi.org/10.1002/esp.3624>
- 910 Sassi, M.G., Hoitink, A.J.F., Vermeulen, B., Hidayat, 2011. Discharge estimation from H-
911 ADCP measurements in a tidal river subject to sidewall effects and a mobile bed. *Water*
912 *Resour. Res.* 47, 1–14. <https://doi.org/10.1029/2010WR009972>
- 913 Shugar, D.H., Clague, J.J., 2011. The sedimentology and geomorphology of rock avalanche
914 deposits on glaciers. *Sedimentology* 58, 1762–1783. <https://doi.org/10.1111/j.1365-3091.2011.01238.x>
- 916 Sime, L.C., Ferguson, R.I., Church, M., 2007. Estimating shear stress from moving boat
917 acoustic Doppler velocity measurements in a large gravel bed river. *Water Resour. Res.*
918 43, 1–12. <https://doi.org/10.1029/2006WR005069>
- 919 Stutenbecker, L., Delunel, R., Schlunegger, F., Silva, T.A., Šegvić, B., Girardclos, S., Bakker,
920 M., Costa, A., Lane, S.N., Loizeau, J.-L., Molnar, P., Akçara, N. and Christl, M., 2018.
921 Reduced sediment supply in a fast eroding landscape? A multi-proxy sediment budget
922 of the upper Rhône basin, Central Alps. *Sedimentary Geology*, 375, 105-19
- 923 Sukhodolov, A.N., Krick, J., Sukhodolova, T.A., Cheng, Z., Rhoads, B.L., Constantinescu,
924 G.S., 2017. Turbulent flow structure at a discordant river confluence: Asymmetric jet
925 dynamics with implications for channel morphology. *J. Geophys. Res. Earth Surf.* 122,
926 1278–1293. <https://doi.org/10.1002/2016JF004126>
- 927 Sukhodolov, A.N., Sukhodolova, T.A., 2019. Dynamics of Flow at Concordant Gravel Bed
928 River Confluences: Effects of Junction Angle and Momentum Flux Ratio. *J. Geophys.*
929 *Res. Earth Surf.* 124, 588–615. <https://doi.org/10.1029/2018JF004648>
- 930 Szupiany, R.N., Amsler, M.L., Best, J.L., Parsons, D.R., 2007. Comparison of fixed- and
931 moving vessel measurements with an aDp in a large river. *Journal of Hydraulic*
932 *Engineering*, 133, 1299–1309.
- 933
934 Tang, W., Hong, J., Huang, X., Huang, J., 2018. Key issues on seepage analysis in mountain
935 river embankment. *IOP Conf. Ser. Earth Environ. Sci.* 189 052041.
936 <https://doi.org/10.1088/1755-1315/189/5/052041>
- 937 Venditti, J., G., Rennie, C.D., Bomhof, J., Bradley, R.W., Little, M., Church, M., 2014. Flow
938 in a bedrock canyon. *Nature*, 513:534-537, <https://doi.org/10.1038/nature13779>.
- 939 Vermeulen, B., Sassi, M.G., Hoitink, A.J.F., 2014b. Improved flow velocity estimates from
940 moving-boat ADCP measurements. *Water Resources Research*, 50, 4186–4196.
- 941
942 Yuan, S., Tang, H., Li, K., Xu, L., Xiao, Y., Gualtieri, C., Rennie, C., Melville, B.
943 Hydrodynamics of a large confluence: Flow, suspended sediment transport

944 andmorphological features. Water Resources Research,
945 <https://doi.org/10.1029/2020WR028284>,2021
946
947 [https://www.bafu.admin.ch/bafu/fr/home/themes/eaux/etat/donnees/statistiques-des-](https://www.bafu.admin.ch/bafu/fr/home/themes/eaux/etat/donnees/statistiques-des-cruces.html)
948 [cruces.html](https://www.bafu.admin.ch/bafu/fr/home/themes/eaux/etat/donnees/statistiques-des-cruces.html)
949